ANKARA YILDIRIM BEYAZIT UNIVERSITY

GRADUATE SCHOOL OF NATURAL AND APPLIED SCIENCES

INVESTIGATION OF THE USE OF POLYPYRROLE AND PEDOT:PSS COATED ELECTROSPUN POLYMER NANOFIBERS AS GAS DIFFUSION LAYER IN PEM FUEL CELLS

M.Sc. Thesis by

Nurcan Aşçı

Department of Materials Engineering

July, 2024

ANKARA

INVESTIGATION OF THE USE OF POLYPYRROLE AND PEDOT:PSS COATED ELECTROSPUN POLYMER NANOFIBERS AS GAS DIFFUSION LAYER IN PEM FUEL CELLS

A Thesis Submitted to

The Graduate School of Natural and Applied Sciences of

Ankara Yıldırım Beyazıt University

In Partial Fulfillment of the Requirements for the Degree of Master of Science in Materials Engineering, Department of Materials Engineering

by

Nurcan Aşçı

July, 2024

ANKARA

M.Sc. THESIS EXAMINATION RESULT FORM

We have read the thesis entitled **"INVESTIGATION OF THE USE OF POLYPYRROLE AND PEDOT:PSS COATED ELECTROSPUN POLYMER NANOFIBERS AS GAS DIFFUSION LAYER IN PEM FUEL CELLS"** completed by **NURCAN AŞÇI** under the supervision of **ASSOC. PROF. ŞERİFE AKKOYUN** and we certify that in our opinion it is fully adequate, in scope and in quality, as a thesis for the degree of Master of Science.

Assoc. Prof. Şerife AKKOYUN

Supervisor

Prof. Dr. Mustafa İLBAŞ

Jury Member

Asst. Prof. İdris Tuğrul GÜLENÇ

Jury Member

Prof. Dr. Sadettin ORHAN

Director

Graduate School of Natural and Applied Sciences

ETHICAL DECLARATION

I hereby declare that, in this thesis which has been prepared in accordance with the Thesis Writing Manual of the Graduate School of Natural and Applied Sciences,

- All data, information and documents are obtained in the framework of academic and ethical rules,
- All information, documents and assessments are presented in accordance with scientific ethics and morals,
- All the materials that have been utilized are fully cited and referenced,
- No change has been made on the utilized materials,
- All the works presented are original,

and in any contrary case of above statements, I accept to renounce all my legal rights.

Date: 24.07.2024 **Signature: ……..**

Name &Surname: Nurcan AŞÇI

ACKNOWLEDGMENTS

I would like to express my sincere gratitude to my supervisor, Assoc. Prof. Şerife AKKOYUN for her guidance, support, and encouragement throughout this research. I am sure that I will move forward by building on her valuable teachings in both my professional and personal life.

I am deeply thankful to my co-supervisor, Prof. Dr. Selahattin ÇELİK for his constructive feedback and suggestions, which greatly enhanced the quality of this work.

Special thanks are also due to Dr. Tolga ALTAN from Niğde Ömer Halisdemir University, and Ömer ERDEMİR from LENTATEK for providing the necessary resources and facilities for conducting this research.

Also, I would like to thank my dear friends İffet Nur AKGÜNDÜZ and Kübra ÖZBEK for being there for me and motivating me in difficult times. Thanks to your friendship and support, this process was more enjoyable and successful.

Finally, I would like to thank my family for their support. Especially my mother, who is always there for me when I shed tears, when I am joyful or when I am afraid. I dedicate all my achievements to her.

Nurcan AŞÇI **2024, 24 July**

INVESTIGATION OF THE USE OF POLYPYRROLE AND PEDOT:PSS COATED ELECTROSPUN POLYMER NANOFIBERS AS GAS DIFFUSION LAYERS IN PEM FUEL CELLS

ABSTRACT

The aim of this study is to produce novel gas difusion layers for proton exchange membrane fuel cells with high performances and consisting entirely of nanofibers without the need of traditional macroporous substrate and microporous layer. Another objective is to overcome the negative impacts of the interface between macroporous substrate and microporous layer inducing some resistance to the system and decreasing the cell performance. For this purpose, polymethyl methacrylate nanofiber mats were produced by electrospinning. These layers were coated with polypyrrole and poly(3,4-ethylenedioxythiophene):polystyrene sulfonate conjugated polymers by oxidative polymerization. Polypyrrole nanofiber gas diffusiın layer and poly(3,4-ethylenedioxythiophene):polystyrene sulfonate nanofiber gas diffusion layer were produced. According to the results, cylindrical and homogeneous polymethyl methacrylate nanofibers were obtained. In polypyrrole nanofiber gas diffusiın layer, the polymethyl methacrylate nanofibers were perfectly well coated by polypyrrole whereas voids are observed at the interface between poly(3,4-ethylenedioxythiophene):polystyrene sulfonate and polymethyl methacrylate nanofibers. Bulk porosity measurements at twenty four hours of water immersion also revealed that no dimensional variation was observed for the novel polypyrrole nanofiber gas diffusiın layer which presents a better dimensional stability in wet conditions. The highest conductivity was obtained for poly(3,4-ethylenedioxythiophene):polystyrene sulfonate nanofiber gas diffusion layer. Cell performance tests revealed a remarkable power density for novel polypyrrole nanofiber gas diffusion layer. For the first time in the literature, high-performance gas diffusion layers totally made of conductive polymer coated nanofibers are proposed as low cost alternatives to commercial systems.

Keywords: Electrospinning, conjugated polymers, proton exchange membrane fuel cells, gas diffusion layers.

POLİPİROL VE PEDOT:PSS KAPLANMIŞ VE ELEKTROEĞİRME YÖNTEMİ İLE ÜRETİLEN POLİMER NANOLİFLERİN PEM TİPİ YAKIT HÜCRELERİNDE GAZ DİFÜZYON KATMANI OLARAK KULLANIMININ ARAŞTIRILMASI

ÖZ

Bu çalışmanın amacı, geleneksel makro gözenekli substrat ve mikro gözenekli katmana ihtiyaç duymadan, proton değişim membranlı yakıt hücreleri için yüksek performanslı ve tamamen nanofiberlerden oluşan yeni gaz difüzyon katmanları üretmektir. Diğer bir amaç, makro gözenekli substrat ve mikro gözenekli katman arasındaki arayüzün sisteme karşı bir miktar direnç oluşturup hücre performansını düşüren olumsuz etkilerinin üstesinden gelmektir. Bu amaçla elektroeğirme yöntemiyle polimetil metakrilat nanofiber matlar üretilmiştir. Bu katmanlar, oksidatif polimerizasyon yoluyla polipirol ve poli(3,4-etilendioksitiyofen):polistiren sülfonat konjuge polimerleri ile kaplanmıştır. Polipirol nanofiber gas difüzyon katmanı ve poli(3,4-etilendioksitiyofen):polistiren sülfonat nanofiber gaz difüzyon katmanı üretilmiştir. Sonuçlara göre, silindirik ve homojen polimetil metakrilat nanoliflerinin elde edildiğini göstermiştir. Polipirol nanofiber gaz difüzyon katmanında, polimetil metakrilat nanofiberleri polipirol ile mükemmel bir şekilde kaplanmıştır, fakat poli(3,4-etilendioksitiyofen):polistiren sülfonat ve polimetil metakrilat nanofiberleri arasındaki arayüzde boşluklar gözlenmiştir. Yirmi dört saatlik suya daldırma sırasında yapılan yığın gözeneklilik ölçümleri, ıslak koşullarda daha iyi boyutsal stabilite sunan yeni polipirol nanofiber gaz difüzyon katmanı için hiçbir boyutsal değişimin gözlemlenmediğini ortaya çıkarmıştır. En yüksek iletkenlik poli(3,4-etilendioksitiyofen):polistiren sülfonat nanofiber gaz difüzyon katmanı için elde edilmiştir. Hücre performans testleri, polipirol nanofiber gaz difüzyon katmanının yüksek bir güç yoğunluğunun olduğunu ortaya çıkarmıştır. Literatürde ilk kez, tamamı iletken polimer kaplı nanoliflerden oluşan yüksek performanslı gaz difüzyon katmanları, ticari sistemlere düşük maliyetli alternatifler olarak önerilmektedir.

Anahtar Kelimeler: Elektroeğirme, iletken polimerler, proton değişim membranlı yakıt hücreleri, gaz difüzyon katmanı.

CONTENTS

NOMENCLATURE

Roman Letter Symbols

C	Carbon
cm	Centimeter
g	Gram
l	Thickness
m	Meter
mA	Milliampere
Md	Dry weight for bulk porosity in g
mW	Milliwatt
Mw	Wet weight for bulk porosity in g
N	Nitrogen
nm	Nanometer
O	Oxygen
s	Area
S	Siemens
t	Time
V	Voltage
Wd	Dry weight for water uptake in g
wt.	Weight
Ww	Wet weight for water uptake in g

Greek Letter Symbols

ε	Bulk porosity
µm	Micrometer
ρ	Resistivity
ρ	Density of pure water

Acronyms

BP	Bipolar plate
CL	Catalyst layer
DMAC	Dimethylacetamide
DMF	Dimethylformamide
EDS	Energy-dispersive X-ray spectroscopy
GDL	Gas diffusion layer

MPL	Microporous layer
MPS	Macroporous layer
MW	Molecular weight
NFGDL	Nanofiber gas diffusion layer
PAN	Polyacrylonitrile
PANI	Polyaniline
PEDOT	Polyethylenedioxythiophene
PEM	Proton exchange membrane
PEMFC	Proton exchange membrane fuel cell
PMMA	Polymethyl methacrylate
PPy	Polypyrrole
PSF	Polysulfone
PSS	Polystyrene sulfonate
PT	Polythiophene
PTFE	Polytetrafluoroethylene
PVA	Polyvinyl alcohol
PVP	Polyvinylpolypyrrolidone
SEM	Scanning electron microscope
TiO_2	Titanium Dioxide
WU	Water uptake

LIST OF TABLES

LIST OF FIGURES

CHAPTER 1

INTRODUCTION

The increase in the world population induces a greater need for energy. Energy from renewable sources or not, powers equipments used in many aspects of daily life such as housing, communication, and transportation. Renewable energy sources are diverse and are classified depending on their origin as solar, wind, or biomass energies. Concerning non-renewable energy sources, coal, natural gas, and oil, are converted into thermal or electrical energy. While the electrical energy generated by electron movement demonstrates a country's presence in defense and the world economy, it also has a significant impact on people's social lives. For this reason, every opportunity available in a country is used to produce electrical energy.

Figure 1.1 shows the shares of different energy sources in the world's energy production in 2021. While the most used resource is coal (35.12%), non-renewable resources are still dominant [1].

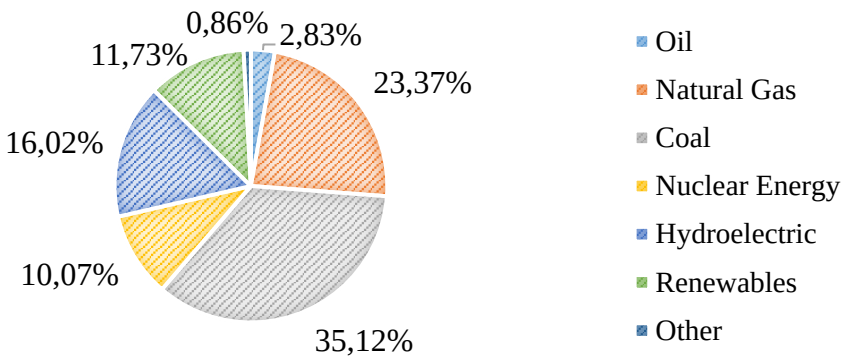

Figure 1.1 Shares of different energy sources in electricity generation of the world in 2021 [1]

Nowadays, although non-renewable energy sources are mainly used for electricity production, their disadvantages such as limited access, rapid consumption, and long production time increase the incentive to use renewable resources [2]. Moreover, it has

bad effects on human health and the environment as greenhouse gases are released during their burning. These gases are dangerous for the ozone layer which traps harmful rays such as ultraviolet rays from the sun, UV-B and UV-C [3]. On the contrary, the reserves of renewable energy resources are constantly renewed by the functioning of nature. If processed, they do not harm nature or human life.

Historically, the foundations of electricity production, discovered by Michael Faraday, an English chemistry and physics scholar, between 1820 and 1830, have survived to this day. Faraday worked on electromagnetic induction and electrolysis and invented the electric motor and dynamo [4]. He also defined the unit of current, the "ampere", and used terms such as "electrolyte", "electrode", "anode", "cathode" and "ion". During his studies, he focused a lot on the fact that electricity appeared in different forms, which revealed new theories about electricity [4].

One of the current emerging technologies for the production of electricity is fuel cells. These energy devices are composed of anode and cathode electrodes separated by an electrolyte. In the first fuel cell model developed by William Robert Grove in 1838 and called the Grove Cell, a zinc electrode immersed in zinc sulfate and a platinum electrode immersed in nitric acid were separated by a porous ceramic pot [5]. A current of 12A and a voltage of around 1.8V were observed with this preliminary device [5]. In 1842, Grove developed a gas voltaic battery that produced electrical energy using hydrogen and oxygen [6]. Another important study was Friedrich Wilhelm Ostwald's experimental determination of the functions of fuel cell components in 1893. These findings, which are the pioneers of many important studies, have contributed to the development of fuel cells and allowed them to gain a place in different fields today.

Fuel cells are systems where the chemical energy is continuously converted into electrical energy under conditions where a fuel and an oxidizer are provided. Although their principle is similar, different types of fuel cells exist. Depending on the nature of their electrolyte, fuel cells are classified as proton exchange (or polymer electrolyte) membrane fuel cell (PEMFC), phosphoric acid fuel cell (PAFC), alkaline fuel cell (AFC), molten carbonate fuel cell (MCFC) or solid oxide fuel cell (SOFC) as illustrated in Figure 1.2.

Basically, the fuel sent to the anode undergoes an oxidation reaction and breaks down into protons and electrons. Protons pass through the electrolyte and electrons circulate through an external circuit to the cathode layer. As a result of the reduction reaction that takes place at the cathode, the oxidant combines with protons and electrons coming from the anode to form water [7].

Fuel cells emit low levels of harmful gases, resulting in almost zero emission values. In addition, since the energy is obtained electrochemically, their efficiency is as high as 60% or above [8]. They are also reliable as they are not affected much by power outages or fluctuations. Hydrogen is usually used as fuel, but gases such as methane, methanol, and ethanol can also be used.

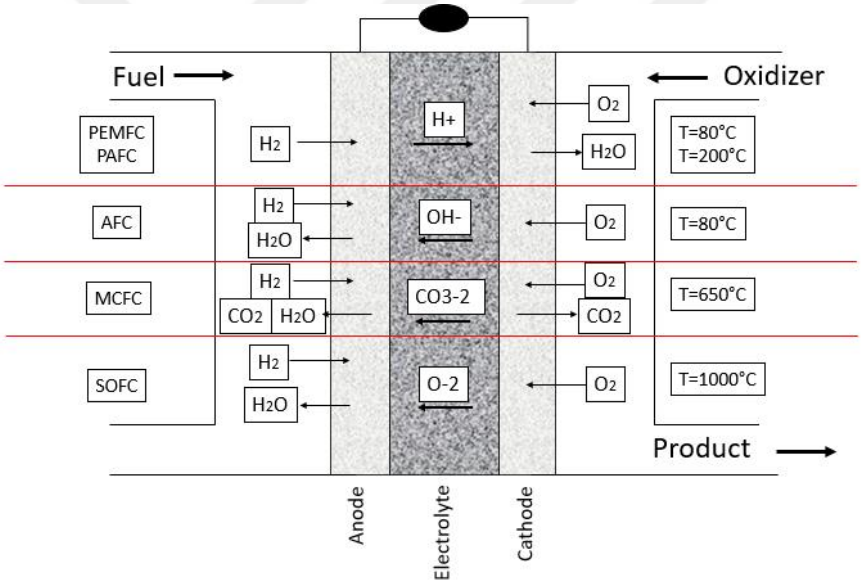

Figure 1.2 Schematic summarizing the different types of fuel cells and their characteristics [9]

Fuel cells can operate at different temperatures and provide energy at different efficiencies allowing their use in various areas. The power ranges of the different fuel cells are presented in Figure 1.3.

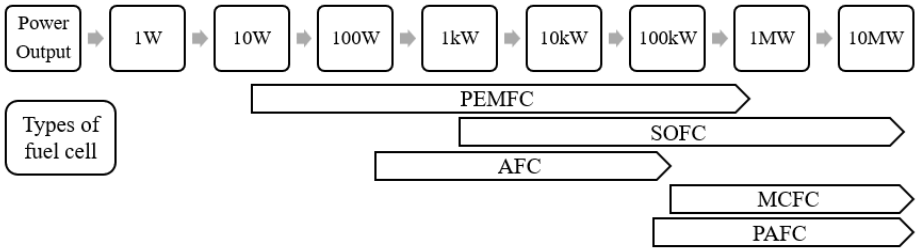

Figure 1.3 Fuel cells and their power ranges [10]

This thesis is particularly focused on proton exchange membrane fuel cells and therefore, the next section is dedicated to PEMFCs to give an overview of these devices.

1.1 Proton Exchange Membrane Fuel Cells (PEMFCs)

Proton exchange membrane (PEM) fuel cells are technological devices that provide electrical energy with high efficiency in clean ways, using hydrogen and oxygen as fuels, which are abundant on earth, and produce only water and heat as waste. PEM fuel cells which stand out with their advantages such as high efficiency obtained at low operating temperature (typically 80°C), with a fast start-up thanks to a simple design and lightweight, have a wide range of application areas such as in hydrogen fuel cell vehicles [11, 12], power supply in portable electronic devices [13, 14] large-scale power generation [15] and energy storage systems [16].

The working principle of PEMFCs is summarized in Figure 1.4. As the Figure indicates, in these devices, the fuel supplied to the system from the anode electrode is hydrogen gas, which is split into protons and electrons [17]. Protons pass through a polymer electrolyte membrane, which gives the device its name. They reach the cathode electrode and reduce oxygen and thus water is formed [17]. The electrons, on the other hand, travel through the external circuit and reach the connected converter [17]. This simple reaction at low operating temperatures increases the probability of choosing the PEM type among fuel cells.

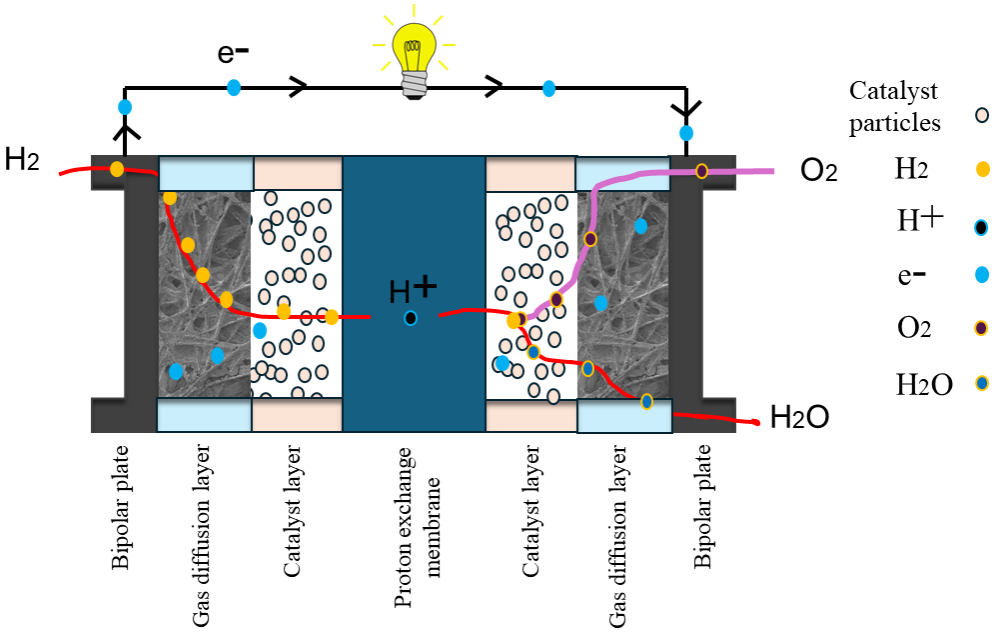

Figure 1.4 Schematic of the working principle of PEMFCs

As mentioned, PEMFCs are composed of an anode and a cathode separated by a porous membrane. Both electrodes are composed of a bipolar plate (BP), a gasket, a gas diffusion layer (GDL), and a catalyst layer (CL) [18]. The membrane only allows protons to pass through, not the electrons. BPs, which are an expensive and heavy component of the system, take part in reactant gas distribution, water transmission, and electrical-thermal conductivity. GDLs are two-layer graded porous components that are between the BPs and CLs. Lastly, the CL, located between the membrane and the GDL, is where the hydrogen oxidation (HOR) and the oxygen reduction (ORR) reactions occur at the anode and cathode, respectively.

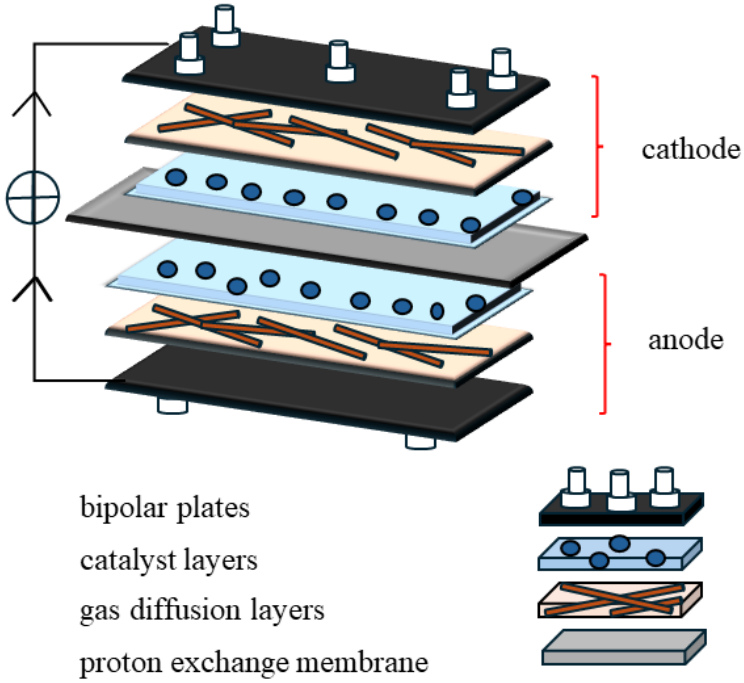

Figure 1.5 Components of a traditional PEMFCs

1.1.1 Bipolar Plates (BPs)

Bipolar plates, which are an expensive and heavy component of the system, take part in reactant gas distribution, water transmission, and electrical-thermal conductivity. Generally, materials such as stainless steel, aluminum, and titanium are used in their production. Besides, the design of the flow field, they act on the diffusion and distribution of the gas in the system, the rate of chemical reactions, the current distribution, and the removal of liquid water [19]. Due to the chemical and physical working conditions they are exposed to, studies are carried out to increase the strength of their structure.

Figure 1.6 shows a comparison of different flow field designs from the literature. The first one (a), shows a design that contains parallel or serpentine plates with capillary columns. Others are a pin type (b), a metal mesh (c), parallel (d), modified (e), single serpentine (f), parallel serpentine (g), mirror serpentine (h), radial (i) and 3D model (j).

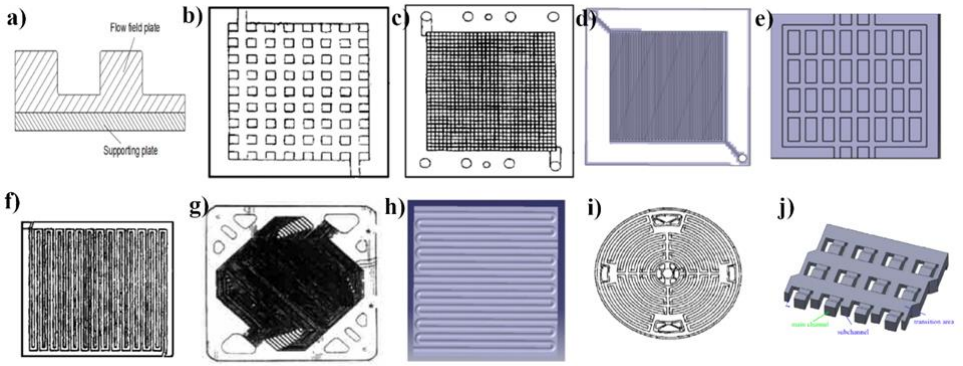

Figure 1.6 Several types of flow field design [8], a) parallel or serpentine plates with a capillary columns [20], b) pin type [21], c) metal mesh [22], d) parallel [23], e) modified [24], f) single serpentine [24], g) parallel serpentine [25], h) mirror serpentine [26], radial [27], j) 3D flow field [28]

1.1.2 Gas Diffusion Layers (GDLs)

GDLs are two-layer graded porous components that are between the bipolar plates and catalyst layers. They are responsible for the homogeneous distribution of reactant gases from the flow field to the anode catalyst layer [19]. They also provide pathways for the produced water and heat from the cathode catalyst layer to the bipolar plates [19]. As this thesis is focused on the replacement of this component by a novel nanofiber layer, this component is detailed in the next section.

1.1.3 Catalyst Layer (CL)

The catalyst layer, located between the membrane and the GDL, is where the hydrogen oxidation reaction (HOR) at the anode and the oxygen reduction reaction (ORR) at the cathode occur. The most commonly used catalyst for PEMFCs is platinum. Small platinum particles with a large surface area are finely dispersed on the surface of the catalyst support, which is commonly made of carbon powder such as Vulcan XC72R by Cabot, Black Pearls BP 2000, Ketjen Black International, or Chevron Shawinigan [29].

1.1.4 Membrane

The membrane, one of the main components of the system, has a porous structure and consists of perfluorocarbonsulfonic acid (PSA) ionomer [30]. It allows hydrogen ions to pass through but not the electrons.

As Figure 1.7 shows, the most used membrane material is Nafion^{TM}, manufactured by Dupont and based on perfluorosulfonylfluoride ethyl-propyl-vinyl ether (PSEPVE).

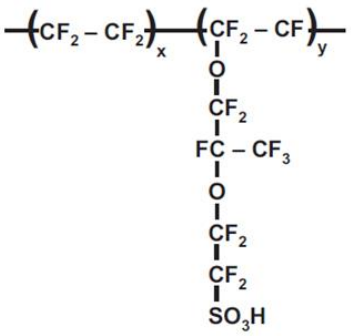

Figure 1.7 Structure of PFSA polymer known as Nafion^{TM} [30]

1.2 A Closer Look at the Gas Diffusion Layers (GDLs)

Basically, a macroporous layer or substrate (MPS) and a microporous layer (MPL) form a GDL's two-layer graded structure [31]. Carbon felt, carbon cloth, carbon fiber paper, and metal-based foams can be used as MPS, but their corrosion is observed in metal-based ones (Figure 1.8).

The most frequently used MPS is carbon fiber paper. Its thickness varies between 200-400 μm and it has a porous structure [19]. It is electrically and thermally conductive and chemically stable. The diameters of the carbon fibers vary between 5-15 μm [19]. Another widely used MPS is carbon fiber cloths. Their structure resembles a woven fabric and they present a high gas permeability and high electrical and thermal conductivities. The characteristics of both MPLs are gathered in Table 1.1.

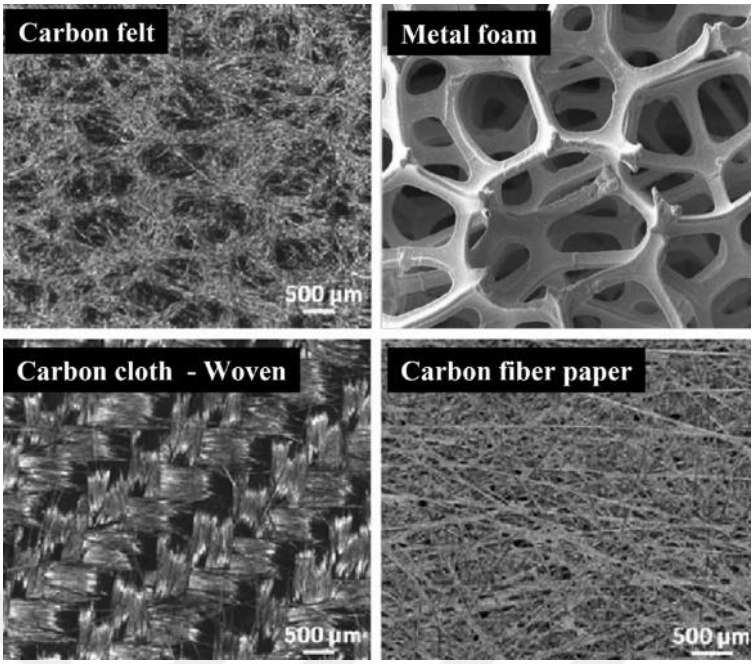

Figure 1.8 Gas diffusion layer substrates [31]

Table 1.1 Features of carbon fiber paper and carbon fiber cloth MPLs

Carbon Fiber Paper	Carbon Fiber Cloth
Thinner, brittle, smoother surface	Thickest, flexible, robust
High electrical/thermal conductivity	High gas permeability and electrical/thermal conductivity
Excellent chemical/thermal stability	Easier to deform and stretch

The MPL consists of materials with conductive carbon particles such as carbon black and graphite and a hydrophobic agent, generally polytetrafluoroethylene(PTFE), that enhances hydrophobicity. Because the pore size of the MPL is substantially smaller than that of the MPS, the airflow entering the CL via the MPL can be controlled with greater homogeneity and the capillarity effect of the micropores in the MPL also aids in the removal of water produced by the cathode reaction [19].

This layer is also applied to reduce the contact resistance between the MPS and the CL. In addition to being a good mechanical support, it also protects the catalyst layer. Moreover, it improves the drainage of water in the cathode as illustrated in Figure 1.9.

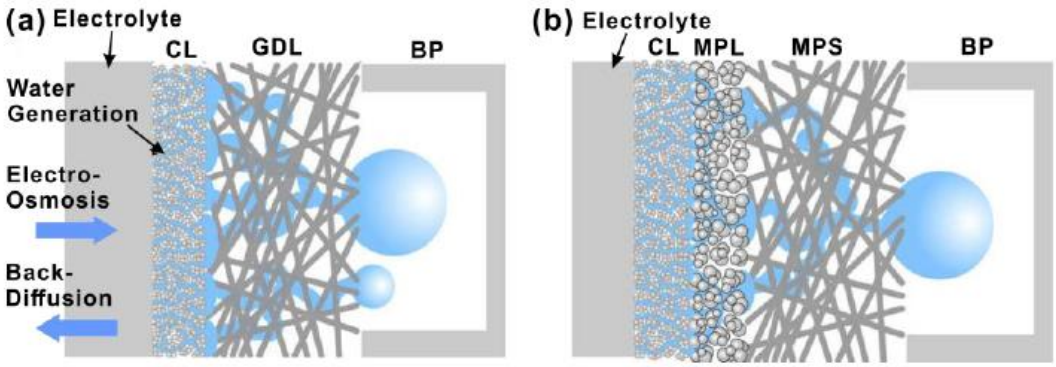

Figure 1.9 Water transport in the cathode: (a) without and (b) with the MPL [19]

1.3 Electrospinning

Polymer nanofibers are recent materials that have caught the attention of many researchers. These novel materials exhibit properties such as high porosity, high surface area, flexibility, strength, lightness, conductivity, or insulation. Thus, nanofiber technology is constantly evolving and the discovery of new applications continues. Among all nanofiber production techniques, electrospinning is the most straightforward and versatile method that allows the obtention of continuous and homogeneous nanofibers with a diameter ranging from few nanometers to a micrometer. As shown in Figure 1.10, the system simply consists of a syringe, a syringe pump, a high-voltage supply, and a metallic collector. The polymer solution to be electrospun is initially charged into a syringe. Then, an electric field is created between the needle and the collector by applying a high voltage. A repulsive electric force opposite to the surface tension is created as the voltage increases and a Taylor cone is formed at the tip of the needle. When the repulsive forces overcome the surface tension, a charged high-speed polymer jet is ejected through the collector. In the meantime, the solvent evaporates as the polymer jet reaches the collector and solid nanofibers are gathered on the collector [32].

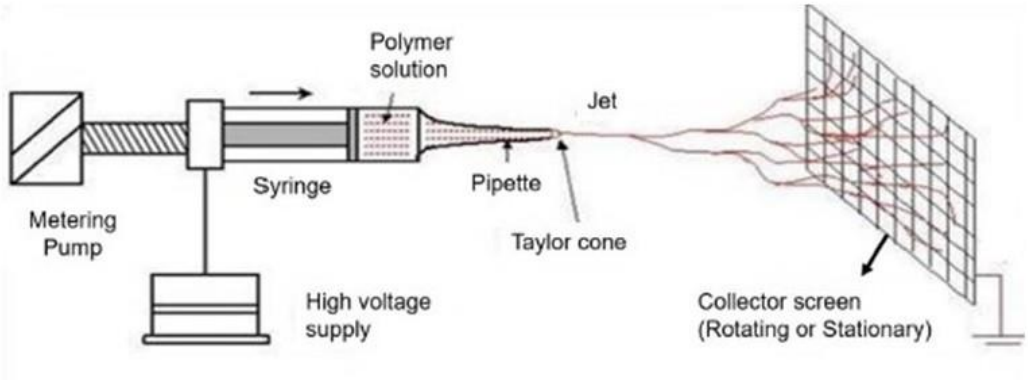

Figure 1.10 Electrospinning of a polymer solution [33]

It is possible to obtain nanofiber structures with different morphologies and properties in electrospinning. These structures can be produced by changing solution parameters such as the viscosity, the polymer concentration, and the polymer molecular weight, ambient parameters such as the relative humidity, and temperature and processing parameters such as the applied high voltage, flow rate, and needle tip-to-collector distance.

The viscosity refers to the resistance of a liquid or fluid to flow. A high-viscosity liquid is a liquid that is dense and has low fluidity.; Such liquids generally flow slowly and consistently. When the viscosity of a polymer solution is too low, the formation of continuous nanofibers does not occur. When the viscosity is too high, it causes hard ejection of jets from the solution. This balance can be improved by controlling the solution concentration or polymer molecular weight [34]. Increasing concentration causes the formation of more uniform and larger diameter nanofibers as shown in Figure 1.11. At low molecular weight, beads may form between cylindrical fibers. As the molecular weight increases, the fiber structure becomes more homogeneous. Nanofibers are formed for polymer concentrations high than a critical concentration [35].

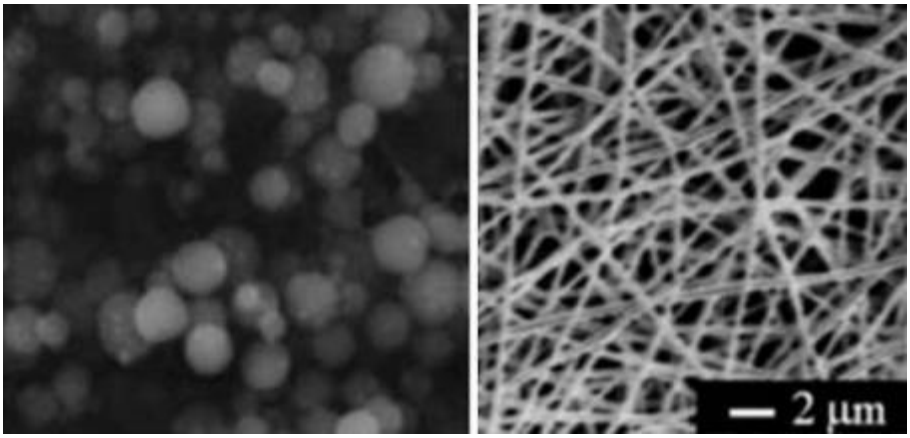

Figure 1.11 SEM images of the electrospun PAN at different concentrations 1.3 and 15 wt. % for the left and right micrographs, respectively. The molecular weight of PAN is 150,000 [34]

The temperature, and humidity are the two most important environmental factors. Excessive temperature in the environment causes an increase in the evaporation rate of the solvent in the solution. When the amount of humidity in the environment increases, the rate of removal of solvents in the solution decreases. Jet initiation depends on voltage, the first processing parameter. Dripping happens when the applied voltage is low because the electrostatic force is not strong enough to overcome the solution droplet's surface tension, preventing the jet from being expanded. The electrospinning process starts when the applied voltage rises because of an increase in electrostatic force, which ultimately results in jet onset. Often, increasing voltage causes a reduction in fiber diameters as can be seen in Figure 1.12.

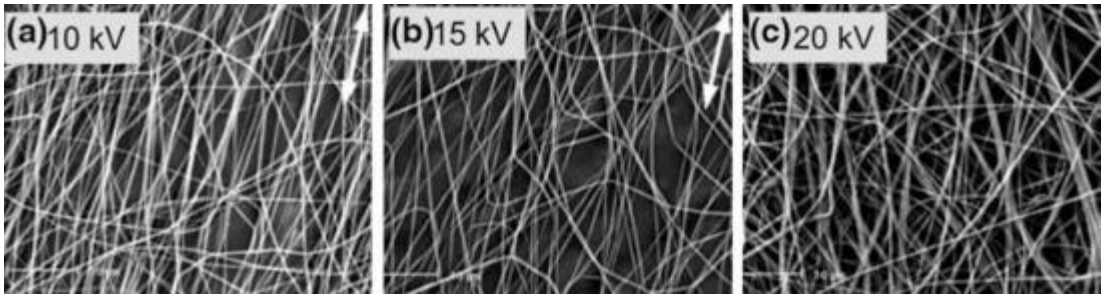

Figure 1.12 SEM images of the ultrafine fibers electrospun from a 20 % PSF solution in DMAC/acetone (9:1) under different voltages. The average fiber diameters are 344 ± 51, 331 ± 26, and 323 ± 22 nm, respectively [36]

The solution flow rate has a significant impact on the properties of the nanofibers. Generally, increasing the flow rate causes an increase in the diameter of the fibers [37]. Nanofiber morphology and structure are affected during the process by the tip-to-collector distance. Too short distance will prevent the fiber from solidifying in time to reach the collector. Beaded nanofibers can be obtained if the distance is too long [38].

Numerous studies on the electrospinning of different polymers such as PMMA [39], PVP [40], PCL [41], TPU [42], PVDF [43], PVA [44], or PVP [45] exist in the literature.

Research and developments in this field enable the use of nanofibers in a wide variety of industrial and scientific fields. Electrospun nanofibers find many potential applications in air [46] and water filtration [47] systems, medical wound dressings [48], energy storage devices [49], textiles [50], electronic circuits [51] and sensors [52].

1.4 Conjugated Polymers

Conducting polymers are new materials with interesting properties as they can present a high electrical conductivity while conserving their thermal insulating characteristic. The existence of conducting polymers was discovered in 1974 [53] and 1977 [54] by H. Shirakawa, A.J. Heeger, and A.G. MacDiarmid's work with polyacetylene. First, the team started researching silver-colored polyacetylene films and observed that the conductivity of these films increased as a result of oxidation. This work earned the team the Nobel Prize in Chemistry in 2000 [55].

Conducting polymers have conjugated double bonds in their main chain, which enable the transmission of electrons along the chain through the alternating σ and π chemical bonds.

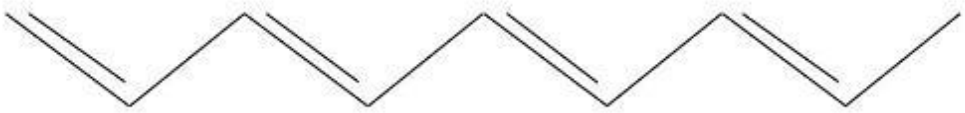

Figure 1.13 Structure of a polyacetylene chain with alternating σ and π bonds

The conductivity of conjugated polymers is increased by the process called doping. In this method, positively charged holes or excess electrons are created in the chain by accepting or donating electrons that will provide conductivity [56]. Chemical materials used for this purpose are called dopants. Dopants affect the number of charge carriers and play an important role in the conductivity of the polymer.

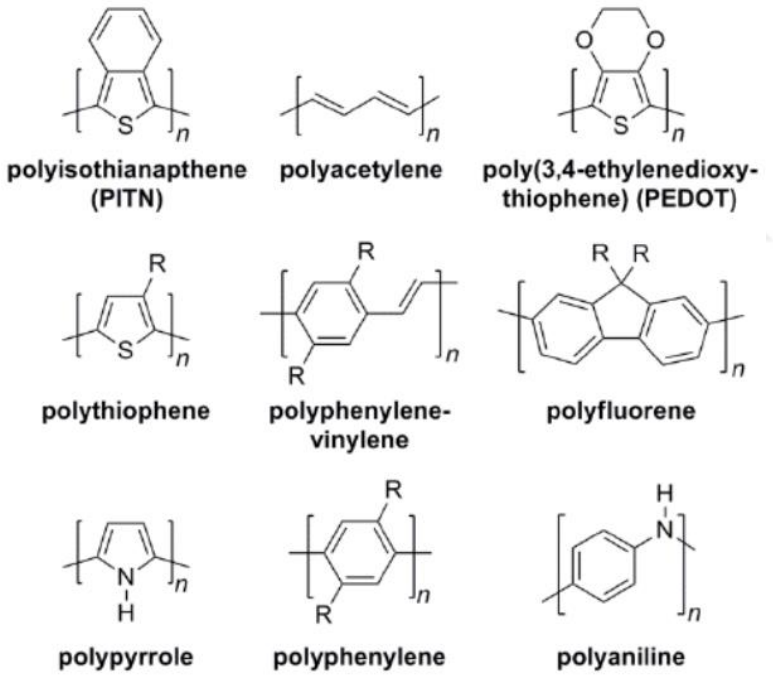

Figure 1.14 Structures of common conjugated polymers [57]

Polypyrrole (PPy), polyaniline (PANI), polythiophene (PT), polyethylenedioxythiophene (PEDOT) are the most common conjugated polymers. These polymers are used in many different areas such as sensors [58, 59], thin films [60], supercapacitors [61], fuel cells [62, 63], and medical drug delivery [64].

PPy is an intrinsically conducting polymer obtained by oxidative polymerization of pyrrole monomer. It changes the color of the surface on which it is applied to dark blue or black as a result of oxidation. It has good structural stability and is easy to synthesize but is insoluble in most organic solvents [65]. PEDOT is obtained as a result of the polymerization of EDOT monomer. Additionally, pure PEDOT is hydrophobic and insoluble in many solvents. Therefore, the presence of a stabilizer or dopant molecule is necessary for its synthesis in water or other solvents [66]. Polystyrene sulfonate (PSS) is a non-conductive hydrophilic polymer surfactant but is used to disperse PEDOT in water or other solvents. Consequently, the outside layer is composed of hydrophilic PSS and the inner core is filled by hydrophobic PEDOT [67]. To sum up, PEDOT:PSS is a combination that is widely chosen since it offers notable benefits in a variety of applications.

Generally, conductive polymers with low molecular weight are difficult to electrospun due to their low solubility in most solvents. Therefore, they are mixed with spinnable agents. Merlini et al. [68], produced non-woven PVDF/PPy mats with highly pressure-sensitive electrical conductivity. In this study, PPy particles with DBSA as the dopant were filled into PVDF at up to 23 wt.% and electrospun. According to the results obtained, the maximum sensitivity was obtained by observing the electrical resistivity decrease in 10 orders of magnitude with the solution mixture containing 13 wt.% PPy by weight. In other words, stress-induced conducting pathways were achieved with the PVDF/PPy electrospun system.

Choi et al. [69], fabricated PEDOT:PSS/PVP nanofibers for organic vapour sensing. In this study, PVP was chosen as a carrier, solution viscosity modifier, and sensing material for detecting organic vapors. Thus, PEDOT:PSS, which will provide conductivity, was blended with PVP and electrospun. According to the results, the average fiber diameters of PEDOT:PSS/PVP and PVP nanofibers were 153.5 and 212 nm, respectively. The electrical conductivity of PEDOT:PSS/PVP nanofibers was 2.34×10^{-12} $S.cm^{-1}$. Additionally, PEDOT:PSS/PVP showed a better organic vapor sensing performance than PVP nanofibers.

1.5 Aim of the Thesis

This thesis aims to develop a conductive and high-performance gas diffusion layer using exclusively a nanofiber structure for PEM fuel cells, eliminating the necessity for microporous and macroporous layer components typically found in traditional GDLs. For this purpose, electrospun polymethylmethacrylate (PMMA, $(C_5H_8O_2)_n$) nanofibers coated with polypyrrole (PPy) and poly(3,4-ethylenedioxythiophene):polystyrene sulfonate (PEDOT:PSS) conductive polymers were first addressed. Electrospinning is a simple method that provides continuous and controlled nanofiber production [70]. It is also expected that due to smaller pores between the nanofibers, the contact surface between the nanofiber GDLs and the membrane is improved. Therefore, the resistance induced by the pores at the interface will reduced thus increasing the performance of the fuel cell. Moreover, the porous structure improves water removal and retention, while nano-sized pores prevent the catalyst particles in the catalyst layer from filling into the GDL pores and clogging in case of any excess pressure. To the best of our knowledge, this study represents a pioneering effort in the field, with potential implications for future research in GDL development.

CHAPTER 2

EXPERIMENTAL

2.1 Materials

Poly(methyl methacrylate) (PMMA, Mitsubishi Chemical Co., V001) was used to produce the electrospun nanofibers. The solvent used is dimethylformamide (DMF), with a density of 0.94 g/cm^3, and was supplied from ISOLAB. Iron(III) chloride hexahydrate ($FeCl_3.6H_2O$, MW: 270.33 g/mol) was purchased from Merck. Pyrrole monomer (MW = 67.09 g/mol), 3,4-ethylenedioxythiophene monomer (MW = 142.18 g/mol), poly(4-styrenesulfonic acid) solution (MW = ~75000 g/mol - 18 wt.% in water), sodium persulfate ($Na_2S_2O_8$) were purchased from Merck. Pyrrole monomer was purified by distillation prior to use. A commercial GDL, SGL28BC (SIGRACET) with 5±1% PTFE load of backing and 23% PTFE content of MPL was used to compare the performances of the novel nanofiber-based GDLs. Epoxy resin and hardener (Epofix) were supplied from Struers. Pure (99.5%) H_2 and O_2 gases were supplied from ANKARAGAZ.

2.2 Production of PMMA nanofiber layers by electrospinning

Firstly, in order to determine the optimal PMMA concentration allowing the obtention of nanofibers by electrospinning, PMMA solutions in DMF of different concentrations were prepared. The optimal PMMA concentration was identified as 3 wt.% of PMMA. Therefore, PMMA solutions of 3 wt.% were prepared by dissolving PMMA pellets in DMF at ambient temperature as illustrated in Figure 2.1. The solutions were maintained under constant stirring until the complete dissolution of PMMA.

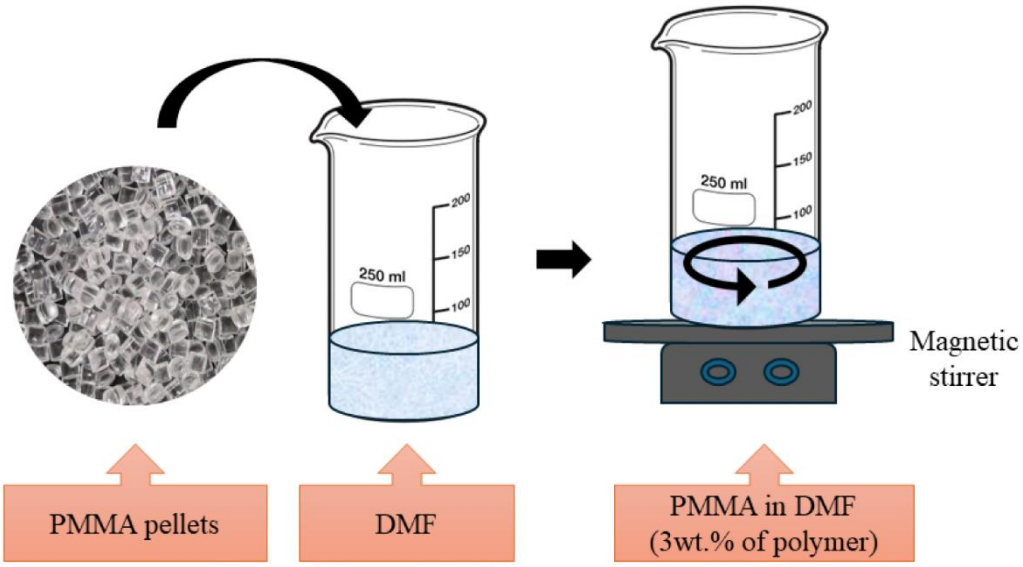

Figure 2.1 Schematic of the preparation of PMMA solutions

Then, the prepared PMMA solutions were electrospun applying a high voltage of 30 kV, a flow rate of 5 mL/h, and a tip-to-collector distance of 30 cm. The nanofiber mats were collected on an aluminum foil for 5 hours (Figure 2.2).

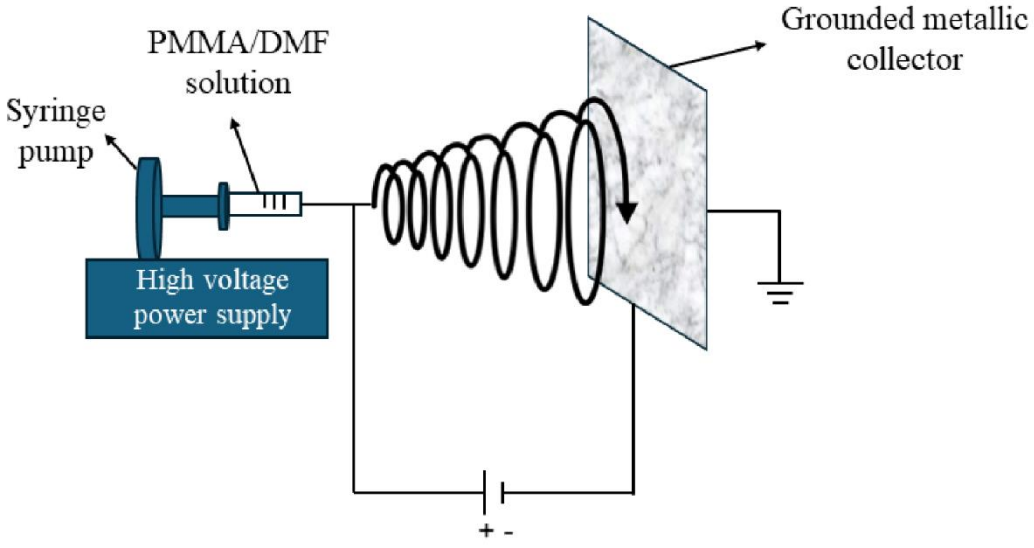

Figure 2.2 Schematic of the electrospinning of PMMA nanofibers

2.3 Preparation of PPy conductive polymer coated nanofiber GDL (PPy-NFGDL)

PMMA is an insulating material. Therefore, in order to provide electrical conductivity to the electrospun PMMA nanofiber layers were coated with polypyrrole (PPy), a conjugated conductive polymer by oxidative polymerization. The whole coating procedure is schematically represented in Figure 2.3.

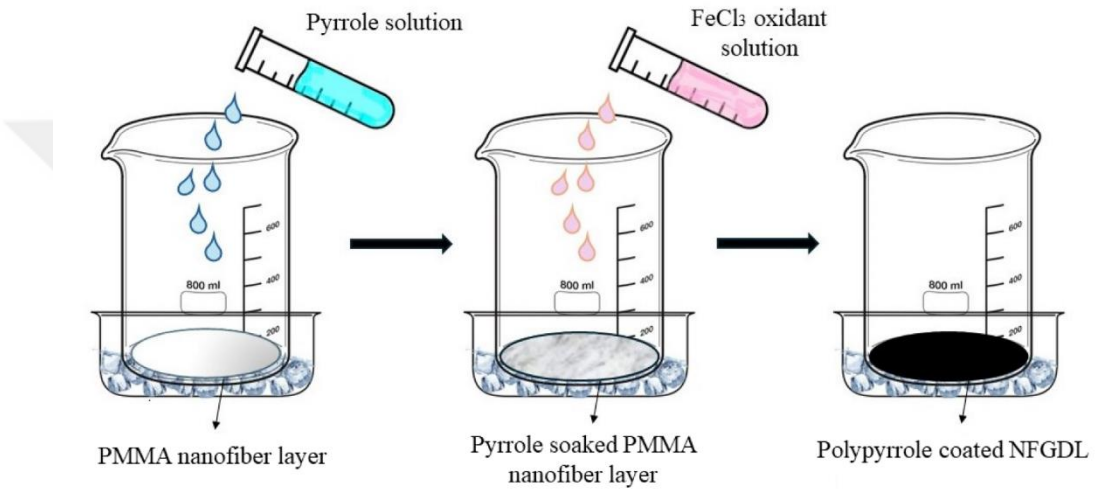

Figure 2.3 PPy coating procedure on PMMA nanofiber as NFGDL

The reaction was conducted as described by Khatti et al. [71], at 4°C. For this purpose, the electrospun PMMA nanofiber mat was first immersed in a 0.25M pyrrole monomer solution and left until complete absorption by the nanofiber layer. Then, a 0.75M $FeCl_3$ oxidant solution was added dropwise in order to initiate the polymerization. As the reaction evolved, the white-colored PMMA nanofiber mat turned dark blue/black which is representative of the formation of polypyrrole polymer (Figure 2.4). Afterwards, the novel NFGDL composed of polypyrrole-coated electrospun PMMA nanofibers was washed with DI water several times and air dried.

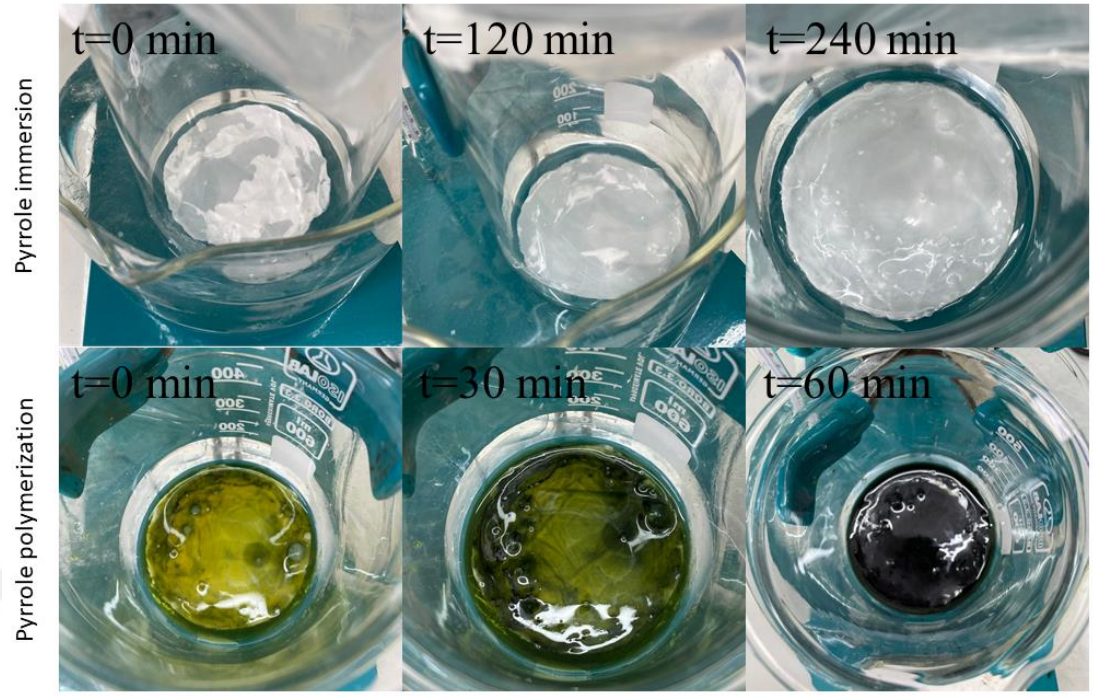

Figure 2.4 Pictures of the PPy-coated NFGDL at different times of the evolution of PPy formation reaction

2.4 Preparation of PEDOT: PSS conductive polymer coated nanofiber GDL (PEDOT: PSS-NFGDL)

In order to prepare the PEDOT:PSS coated NFGDL, the polymerization reaction of the PEDOT:PSS polymer was conducted by modification and adaptation of the method proposed by Sakunpongpitiporn et al. [72]. The whole process is given schematically in Figure 2.5.

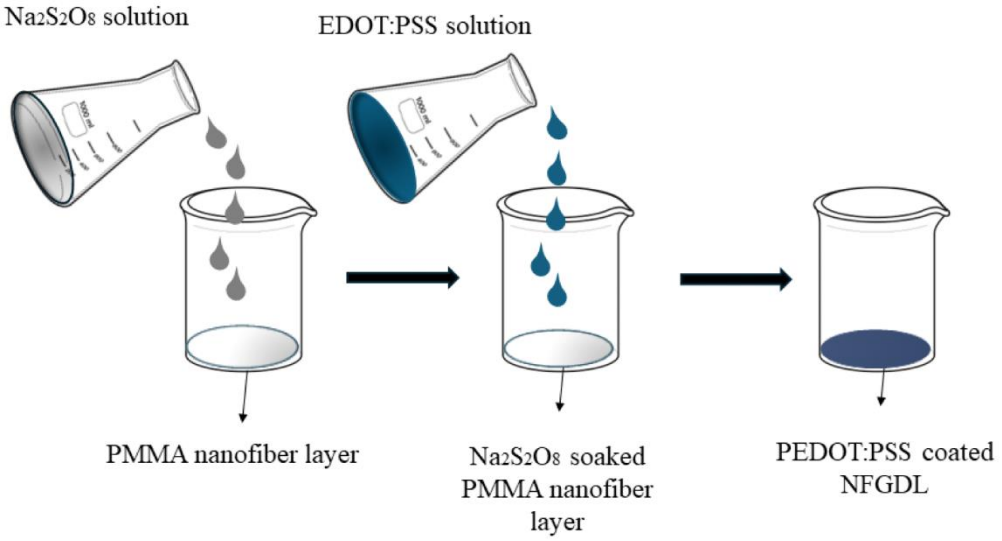

Figure 2.5 PEDOT:PSS coating procedure on PMMA nanofiber as NFGDL

The reaction was conducted at ambient temperature. Similarly to the case of polypyrrole, the electrospun PMMA nanofiber layer was first immersed in $Na_2S_2O_8$ oxidant solution with a $Na_2S_2O_8$:EDOT molar ratio of 2:1. The mat was left for approximately 2 hours to fully absorb the oxidant. Then, the solution with an EDOT:PSS weight ratio of 1:11 was mixed in a magnetic stirrer for a few minutes. At the end of the period, the EDOT:PSS solution was poured dropwise onto the PMMA nanofiber which immersed the oxidant. After waiting 24 hours for the polymerization to complete, the sample was washed with plenty of DI water and left to dry. Pictures of the PEDOT:PSS-coated NFGDL are provided in Figure 2.6.

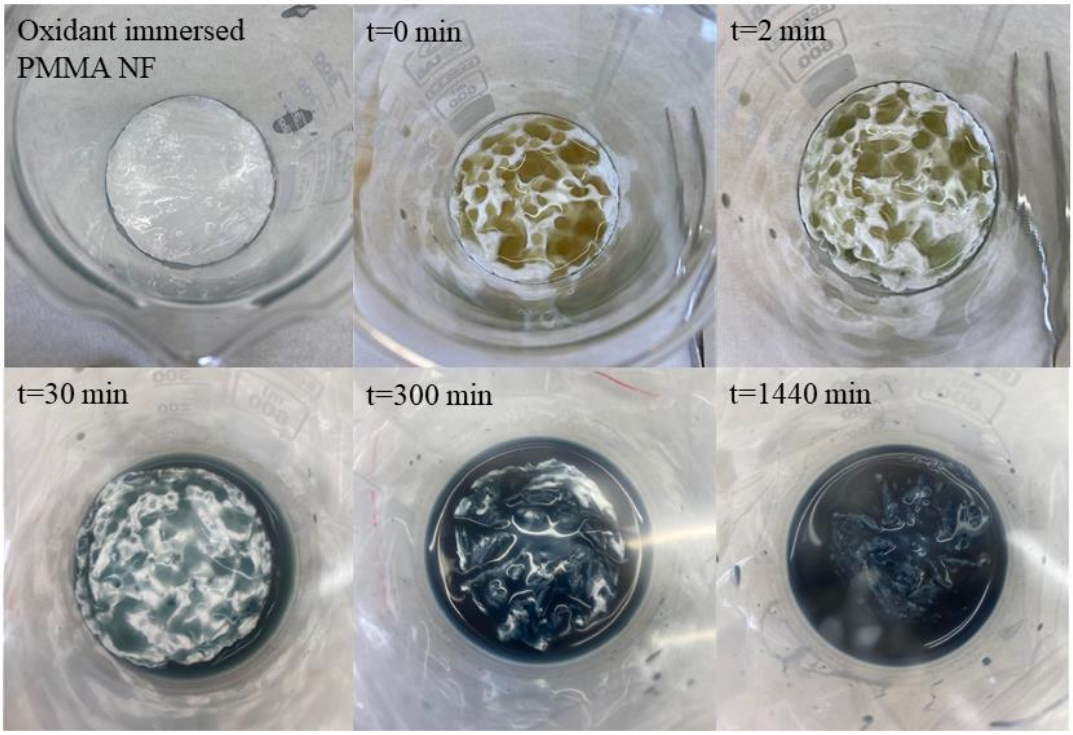

Figure 2.6 Pictures of the PEDOT:PSS-NFGDL at different times of the evolution of PEDOT:PSS formation reaction

2.5 Characterization

2.5.1 Morphological and structural analysis

The morphology and structure of the samples were examined using a HITACHI SU5000 field emission scanning electron microscope (SEM) equipped with an Oxford X-MaxN 80 energy-dispersive X-ray detector (EDS). The average fiber diameters and thicknesses of the samples were determined with ImageJ software (NIH-USA) using the SEM micrographs from 100 nanofibers. The thickness of the samples was determined from the transversal section of the NFGDLs sandwiched between two square PMMA blocks. For each sample, measurements were taken from 10 different areas. The conjugated polymer-coated nanofiber GDL was also embedded in an epoxy resin as illustrated in Figure 3.8 and the transversal section was observed. The resin:hardener ratio used was 25:3 as suggested by the supplier. In order to get a better observation of the position of the conjugated polymers at the surface of the PMMA

nanofibers, the elemental mapping of the transversal sections of NFGDLs were acquired.

2.5.2 Electrical conductivity measurements

The conductivity of the novel nanofiber GDLs was measured using a Keithley 2400 source meter equipped with a Signatone Pro4 four-point probe. For each sample, the measurements were repeated ten times at ten different points.

2.5.3 Water uptake measurements

Water uptake measurements were performed as proposed in [73]. All samples were dried in an oven for 24h until they reached a constant weight prior to the determination of the dry weight of all GDLs. Then, all samples were immersed in DI water and weighed regularly for 24h. Therefore, the time-dependent water uptake (WU) was calculated using Eq. (1) [73].

$$\mathrm{WU\ (t)\ (\%)} = \frac{\mathrm{Ww(t) - Wd}}{\mathrm{Wd}} \times 100 \qquad \textbf{(2.1)}$$

where *Wd* is the dry weight and *Ww*(t) time dependent wet weight of the samples.

2.5.4 Bulk porosity measurements

The bulk porosity measurements were realized on samples of 1×2cm^2 for SGL28BC and PPy-NFGDL, and 0.5×1 cm^2 for PEDOT:PSS-NFGDL. The samples were first immersed in DI water for 10 min and the wet weight was measured. In order to assess the dimensional stability of the nanofiber GDLs under a wet environment, the samples were also weighed after 24h of immersion in DI water. Then, the samples were dried until they reached a constant weight in an oven at 50°C, for 24h, and the dry weight was measured. The bulk porosity was calculated using Eq. (2) [74, 75]:

$$P(\%) = \frac{(W_w - W_d)}{Sl\rho_w} \times 100 \qquad \textbf{(2.2)}$$

where, ρ_w is the density of pure water in g.cm^{-3}, l is the membrane thickness in cm, and S is the membrane area in cm^2.

2.5.5 Performance testing

Figure 2.7 presents of the cell designed for the performance testing of the commercial GDL, and PPy-NFGDL.

In general, the components included in the cell are: graphite bipolar plates, PTFE gaskets, GDLs to be tested, and catalyst-coated membrane. Samples were inserted into the anode cell to conduct performance tests. The cathode cell contains commercial SGL28BC, whose regime is well-known. Neverthless, in order to make comparison and obtain the performance graph, SGL28BC was tested by placing both the anode and cathode in the cell. PPy-NFGDL was placed in the anode part of the cell with SGL28BC in the cathode part and its change in performance was examined.

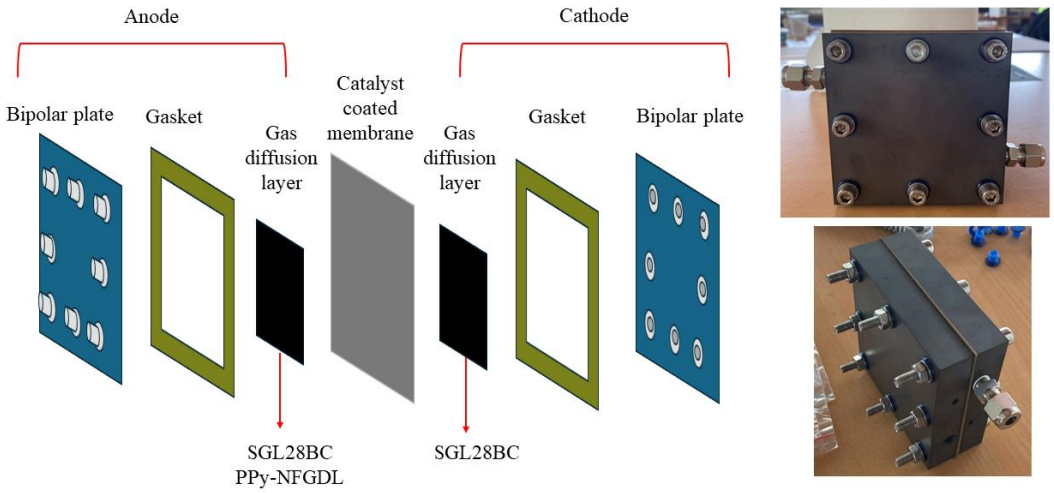

Figure 2.7 Schematic representation of the cell and pictures of the closed cell

Then, performance measurements were realized employing a BK Precision 8524 DC Electronic Load power supply with the cell operating at 25°C. Hydrogen was supplied to the anode, while air was supplied to the cathode. Current values corresponding to different voltages were recorded for both PPy-NFGDL and commercial GDL. Therefore, I-V and current density curves were drawn for both samples.

CHAPTER 3

RESULTS AND DISCUSSIONS

3.1 Morphological analysis and interfaces

The pictures of the commercial GDL (both macroporous substrate (MPS) and microporous layer (MPL) faces), the PMMA nanofiber layer, and the novel conjugated polymer-coated two nanofiber GDLs are presented in Figure 3.1. As shown, the white-colored PMMA nanofiber layer takes on a black color when coated with polypyrrole or a dark blue/black color when coated by PEDOT:PSS conjugated polymers. As it can be noticed, a significant shrinkage in observed in the case of the PEDOT:PSS nanofiber novel GDL sample. This phenomenon was also observed by Valtakari et al. [76] who investigated the effect of different casting methods on the conductivity of PEDOT:PSS containing nanofibrillar cellulose thin films. The authors showed that shrinkage occurred during spin coating and annealing and they attributed it to the compression and fast evaporation of water from the films. This situation is in correlation with our observations as the PEDOT:PSS-NFGDL shrank and became brittle after the drying process. According to the literature [77, 78, 79], the shrinkage of PEDOT:PSS polymer is related to the shrinkage of the hydrophilic PSS polymer chains after evaporation of water.

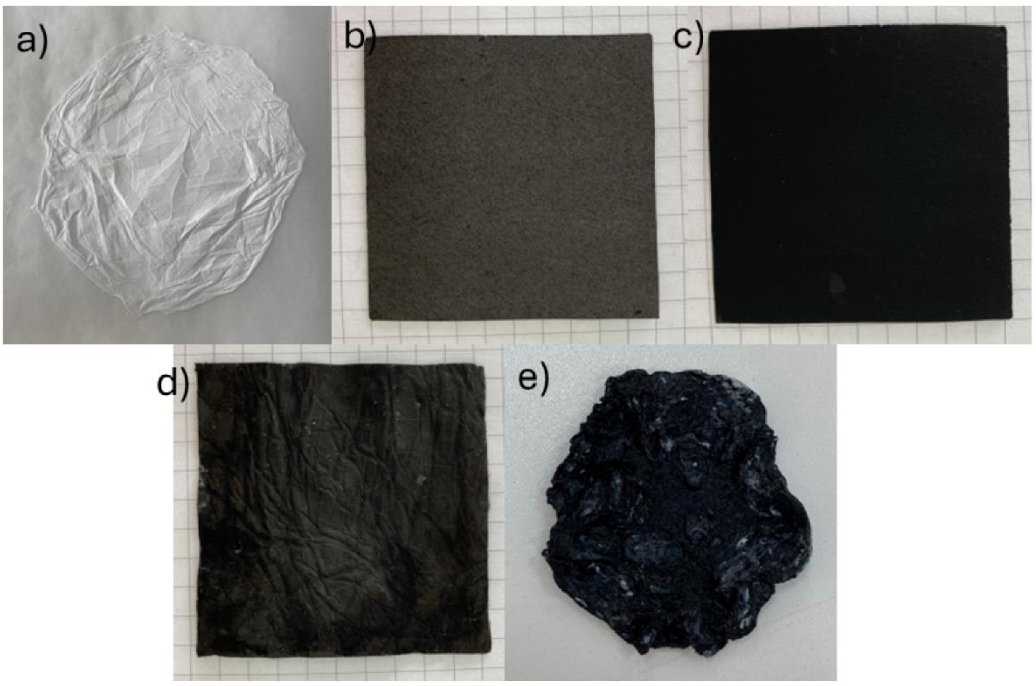

Figure 3.1 Pictures of a) PMMA nanofiber layer, b) SGL28BC macroporous layer, c) SGL28BC microporous layer, d) PPy-NFGDL and e) PEDOT:PSS-NFGDL

Figure 3.2 shows the SEM micrographs of commercial SGL28BC macroporous and microporous layers. The diameter distribution of the PTFE embedded carbon fibers composing the macroporous layer (MPS) is also provided as inset. The results show a wide diameter distribution and an average diameter of 12 µm. This is due to the accumulation of PTFE between the carbon fibers. Similarly, in the study of Carrigy et al. [80], PTFE tends to accumulate in the pores between the carbon fibers of a commercial GDL, thus reducing the pore size. Concerning the MPL structure, many cracks are present at the surface composed of the stacking of PTFE-impregnated carbon particles.

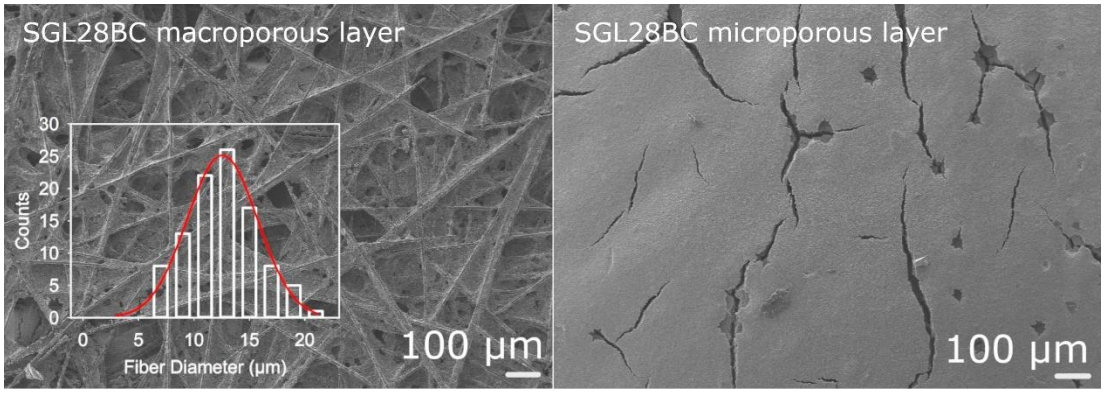

Figure 3.2 SEM micrographs of macroporous and microporous layers of SGL28BC. The fiber diameter distribution of the MPS is also provided as an inset

The SEM micrographs of the PMMA nanofiber layer and novel nanofiber GDLs, PPy-NFGDL and PEDOT:PSS-NFGDL, and the corresponding nanofiber diameter distributions can be seen in Figure 3.3. The results point out that, cylindrical and homogeneous PMMA nanofibers with an average diameter of 696nm were produced. Interestingly, in the case of PPy-NFGDL, the nanofibers have a granular surface and PPy particles polymerized at the surface of the nanofibers are clearly discernable. The average diameters of PPy-NFGDL nanofibers are determined as 798 nm. As expected, after the polymerization of PPy on the nanofibers, the average diameter increases by approximately 100nm. This result seems coherent as the polypyrrole particles synthesized by oxidative polymerization using the same oxidant in a previous study of our group [81] were about 113nm and a wide nanofiber distribution was obtained. After the polymerization of pyrrole onto the PMMA nanofiber mat, the coating did not occlude the pores between PMMA nanofibers. Instead, PPy particles were found to accumulate predominantly on the nanofibers. Similar results were observed by Oroumei et al. [82]. Similarly, the authors produced electrospun PAN nanofibers coated with polypyrrole by in situ chemical oxidative polymerization. PPy particles are located on the nanofiber walls and do not obstruct the pores and the average fiber diameter is between 300-700 nm. On the contrary, the PEDOT:PSS-NFGDL nanofibers do not present a granular surface. They have an average diameter of 717nm. A closer look to the micrograph shows that PEDOT:PSS has not only polymerized on the nanofibers but it also fills the pores between the nanofibers.

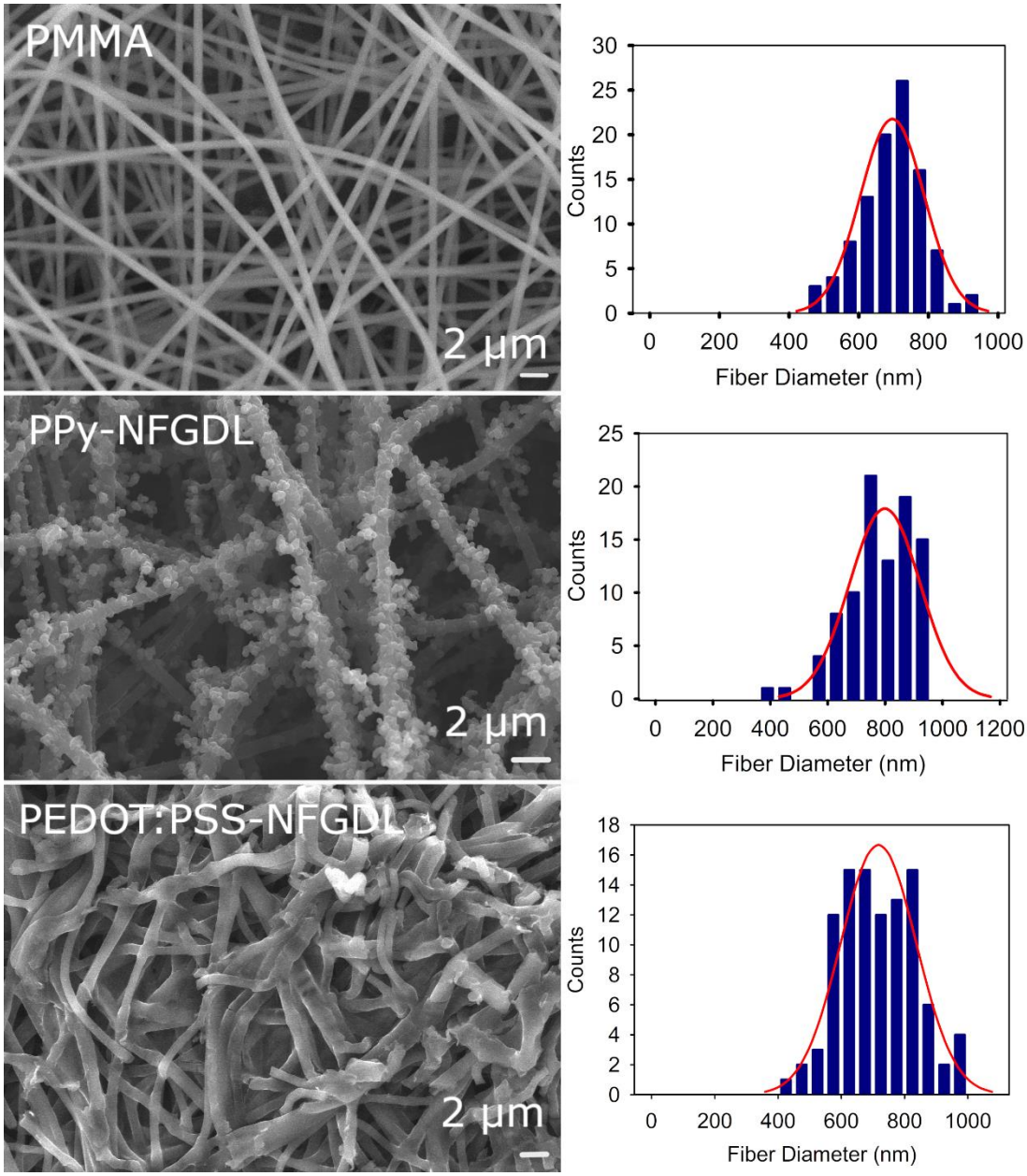

Figure 3.3 SEM micrographs and respective nanofiber diameter distributions of PMMA nanofiber layer, the novel PPy-NFGDL and PEDOT:PSS-NFGDL

In order to determine the thickness of the GDLs, the samples were sandwiched between two PMMA blocks covered by an aluminum tape. The SEM micrographs of their section are presented in Figure 3.4.

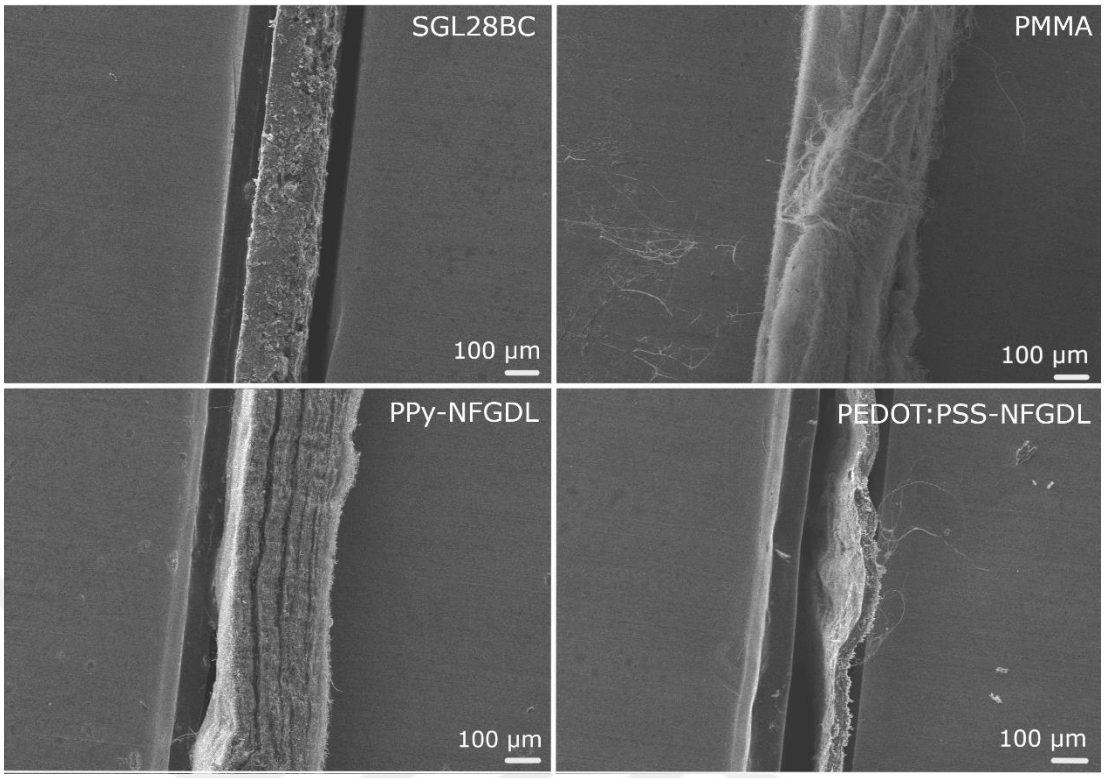

Figure 3.4 SEM micrographs of the sections of SGL28BC, PMMA nanofiber layer, PPy-NFGDL, and PEDOT:PSS-NFGDL

The thickness of the different samples is given in Table 3.1. According to these results, the commercial GDL and the uncoated PMMA nanofiber layer have a thickness of around 200µm and 450µm, respectively. Interestingly, although both conductive polymer-coated nanofiber GDLs are thinner compared to the unfilled PMMA layer, the PEDOT:PSS coated nanofiber GDL is nearly ten fold thinner. Actually, this result seems in correlation with the interpretations given in the morphological analyses section. Indeed, shrinkage was observed in the case of PEDOT:PSS-NFGDL which was attributed to the shrinkage of the PSS segments of the conjugated polymer chain during water evaporation [77, 78, 79].

According to Morgan et al. [83], in situations with high current densities, the GDL should be as thin as possible while with low current densities or dry-humidified systems, a thicker GDL can help regulate the water content more effectively. As a result, it can be said that PPy-NFGDL is appropriate for systems requiring low current

density and PEDOT:PSS-NFGDL is appropriate for scenarios requiring high current density.

Table 3.1 Thicknesses of the samples

Samples	**Thickness (µm)**
SGL28BC	204 ± 1.40
PMMA nanofiber layer	445 ± 19.0
PPy-NFGDL	350 ± 24.0
PEDOT:PSS-NFGDL	48 ± 4.40

The interface between two polymers; PMMA composing the core and PPy or PEDOT:PSS forming the shell of the novel nanofiber GDLs were also investigated. For this purpose, the SEM micrographs of the cross-sections of the PPy-NFGDL and PEDOT:PSS-NFGDL are presented in Figure 3.5. As shown, in the case of PPy-coated NFGDL, the polypyrrole conductive polymer (black arrows) perfectly adheres to the surface of the PMMA nanofiber (red arrows). No gap is observed between the to polymers which seem to be quite compatible. The image also confirms that the granular surface totally covers the PMMA nanofibers as exposed in the morphological analysis section. On the other hand, noticeable gaps pointed out by blue arrows are present between PMMA nanofibers (red arrows) and PEDOT:PSS (green arrows) for the PEDOT:PSS-NFGDL. The conductive polymer not only entrapped the PMMA nanofibers but also filled the pores between the nanofibers as a matrix.

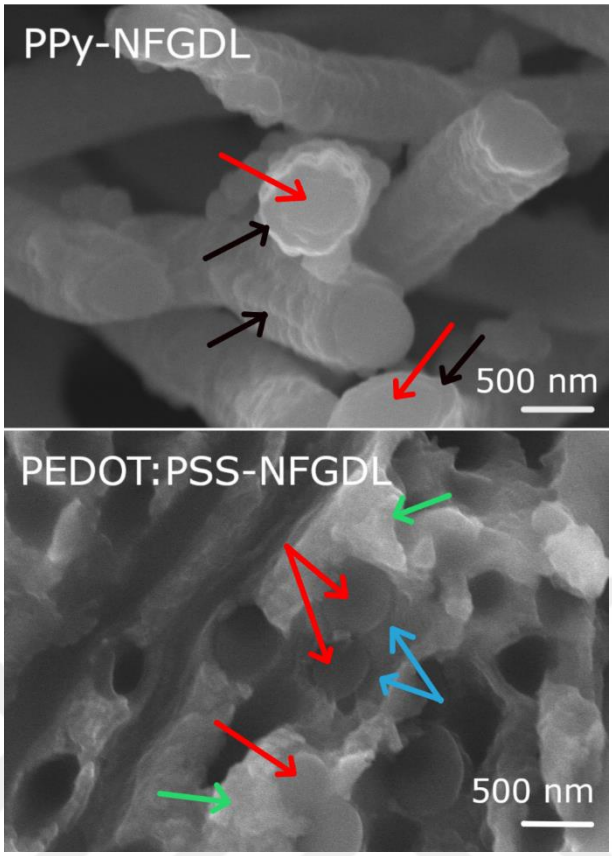

Figure 3.5 SEM micrographs of the cross-section of PPy-NFGDL and PEDOT:PSS-NFGDL showing the interfaces between PMMA nanofibers and conjugated polymers PPy and PEDOT:PSS. Arrows point out PMMA nanofibers (red), PPy (black), PEDOT:PSS (green), and the interfacial gaps (blue) between PMMA nanofibers and PEDOT:PSS

3.2 Structural analysis

In order to clearly localize the conductive polymers PPy and PEDOT:PSS into the nanofiber GDLs, EDS elemental maps of the cross-sections of the nanofibers GDLs were also captured. As shown in Figure 3.6, PMMA, polypyrrole and PEDOT:PSS are polymers and precisely organic materials, they are principally composed of carbon (C), oxygen (O), and hydrogen (H) atoms. However, nitrogen (N) and sulfur (S) atoms are extra atoms that differentiate PPy and PEDOT:PSS, respectively.

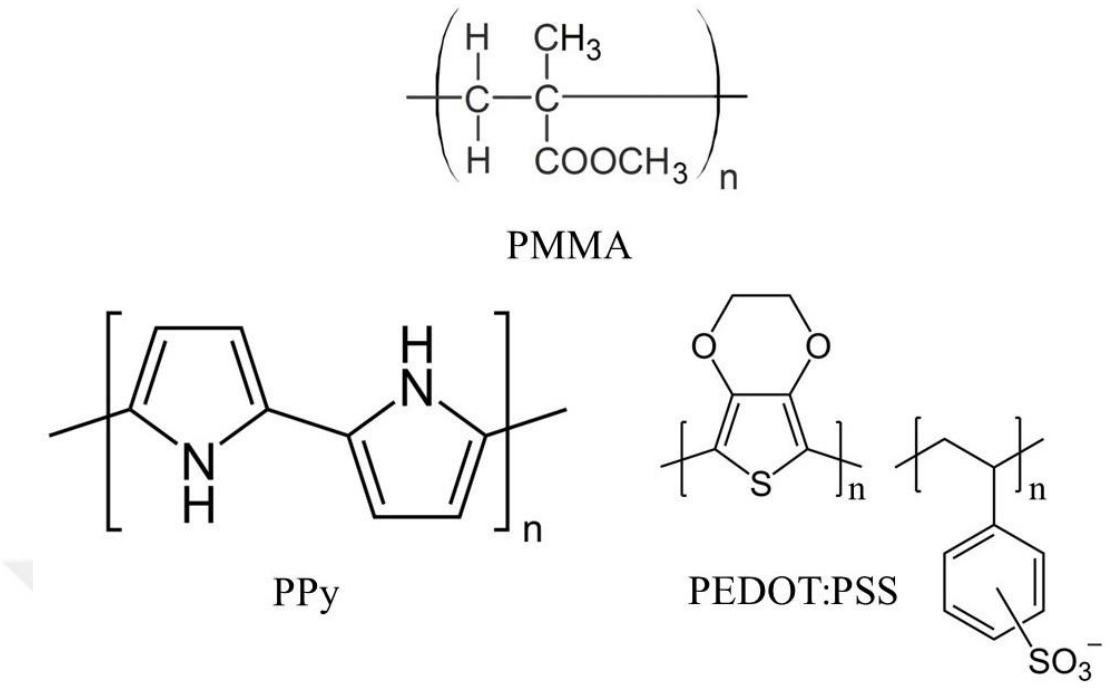

Figure 3.6 Chemical structures of PMMA, polypyrrole, and PEDOT:PSS polymers

Figure 3.7 shows the EDS elemental maps of PPy-NFGDL. Carbon (C) belongs to PMMA and PPy, while oxygen (O) is found in PMMA. The presence of aluminum (Al) is ascribed to the Al tape used to fix the samples. However, although a significant amount of nitrogen (N), which is only found in the structure of PPy, was detected, its localization, is not clearly discernable even in the discrete color image. This is attributed to the presence of important height differences on the analyzed surface as it can be seen on the inset image.

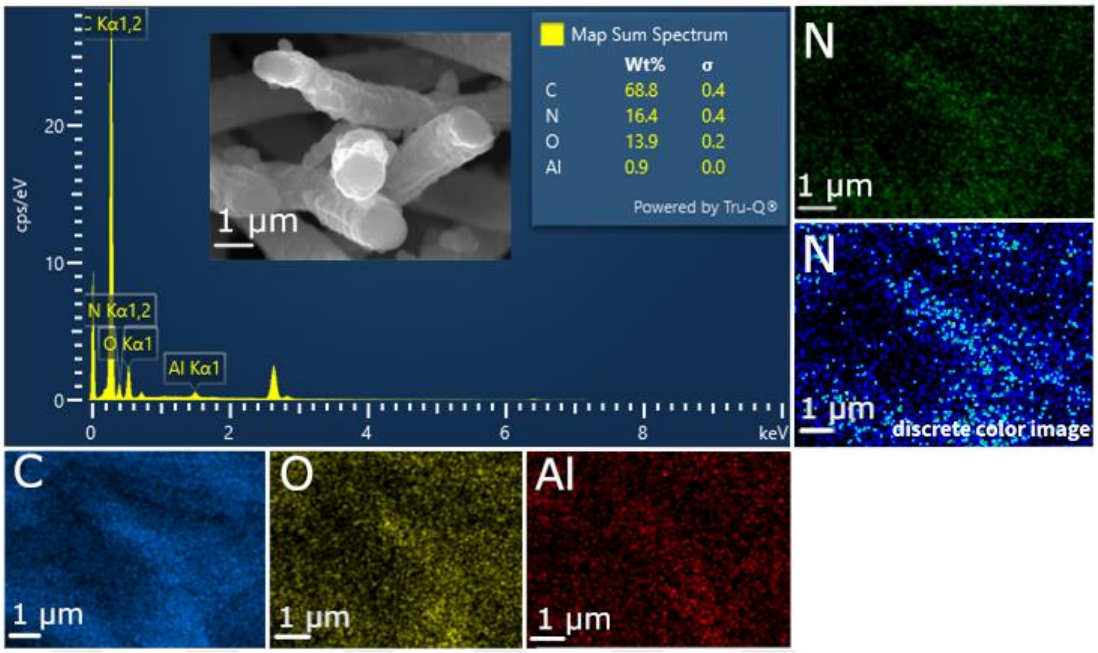

Figure 3.7 EDS spectrum, corresponding elemental composition, and mapping of the cross-section of PPy-NFGDL. The discrete color image is also provided for nitrogen (N)

Therefore, to get a better point of view on the localization of PPy around PMMA nanofibers, the PPy-NFGDL was embedded in epoxy resin as shown in Figure 3.8 and the cross-section was analyzed by EDS.

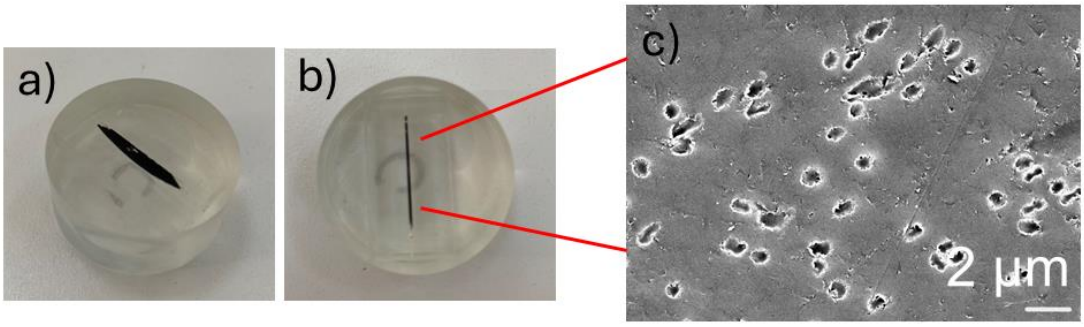

Figure 3.8 Pictures of a) the lateral view, b) the top view and c) SEM micrograph of the section of the PPy-NFGDL embedded in epoxy resin

The EDS results of the epoxy-embedded PPy-NFGDL are given in Figure 3.9. As expected, the analysis area provided as an inset shows a relatively smooth surface. As

the epoxy resin is insulating, the sample was coated with gold prior to analysis. Therefore, the presence of gold (Au) is ascribed to the coating. Aluminum is attributed to the Al tape used to fix the samples. Principal elements composing PMMA and PPy, carbon (C), and oxygen (O) were also detected. Interestingly, nitrogen (N) particularly encircles the PMMA nanofibers either in the elemental map and discrete color image of N. These results clearly confirm the previous interfacial analysis and emphasize that PMMA nanofibers are totally coated by PPy conductive polymer in the PPy-NFGDL.

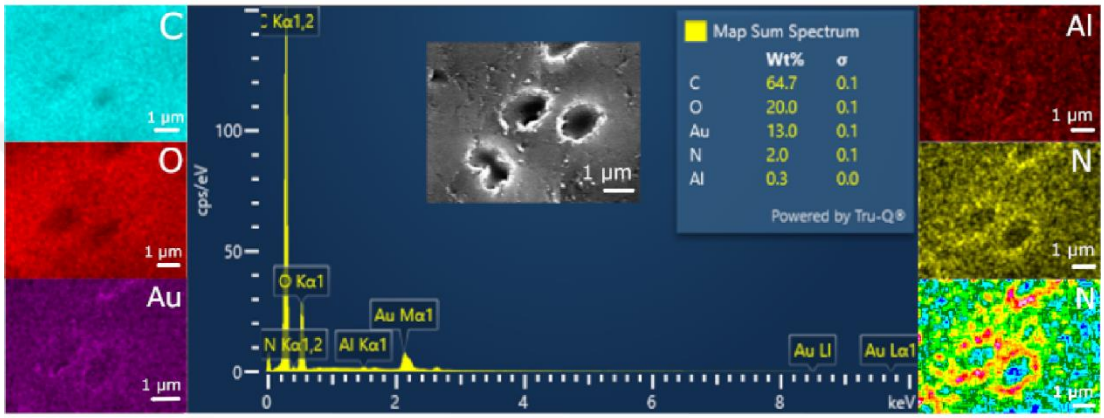

Figure 3.9 EDS spectrum, corresponding elemental composition and mapping of the cross-section of epoxy embedded PPy-NFGDL. The discrete color image is also provided for nitrogen (N)

Similarly, the EDS analysis results of the PEDOT:PSS-NFGDL are given in Figure 3.10. The analysis area is given as an inset. In addition, a discrete color image map of S also is provided. Carbon (C) and oxygen (O), the main atoms of both PMMA and PEDOT:PSS were detected. Aluminum (Al) is also attributed to the aluminum tape used to mount the samples. As developed in the previous section on the morphological analysis and interfaces, contrary to PPy, PEDOT:PSS polymerized not only at the surface of PMMA nanofibers but also occupies the pores between the nanofibers. As expected, the localization of the characteristic element allowing to distinguish PEDOT:PSS, sulfur (S) covers nearly all the surface of the cross-section in both the elemental map and the discrete color image of S.

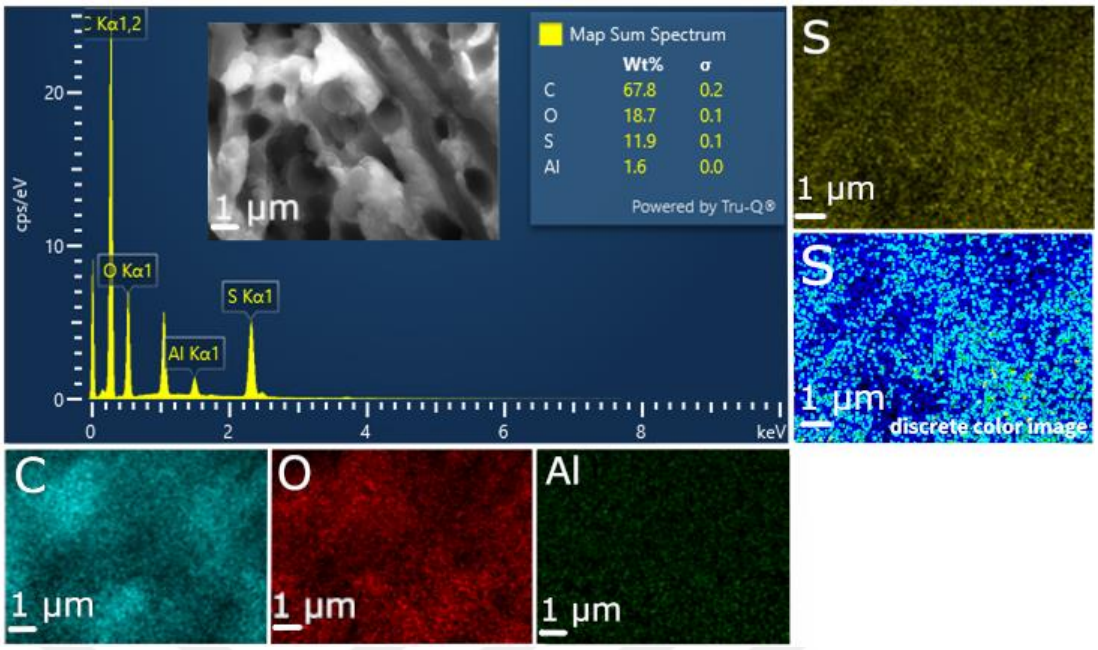

Figure 3.10 EDS spectrum, corresponding elemental composition, and mapping of the cross-section of PEDOT:PSS-NFGDL. The discrete color image is also provided for sulphur (S)

3.3 Water uptake, bulk porosity and dimensional stability of the novel nanofiber GDLs under wet conditions

The time-dependent water uptake (WU) results for SGL28BC, PPy-NFGDL, and PEDOT:PSS-NFGDL are provided in Figures 3.11 and 3.12. The water uptake refers to the water absorption capacity of a material. It may vary depending on factors such as the chemical structure of the material, surface area, and porosity [84, 85]. These Figures show that for all samples, the water uptake is stabilized after nearly ten hours. Although it is about 5% for the commercial SGL28BC, it is much more higher for the nanofiber GDLs, PPy-NFGDL and PEDOT:PSS-NFGDL for which it reaches 700% and 2200%, respectively. The lower WU value of SGL28BC is attributed to the hydrophobic PTFE treatment applied to the MPS and MPL layers of commercial GDLs, despite having a porous structure. In PPy-NFGDL and PEDOT:PSS-NFGDL, the matrix phase consists of PMMA. Hydrophilic polymers such as PMMA tend to absorb water, increasing water uptake. Additionally, having a nanofiber structure, they

have a high surface area, so they can absorb more water because water molecules have more contact points.

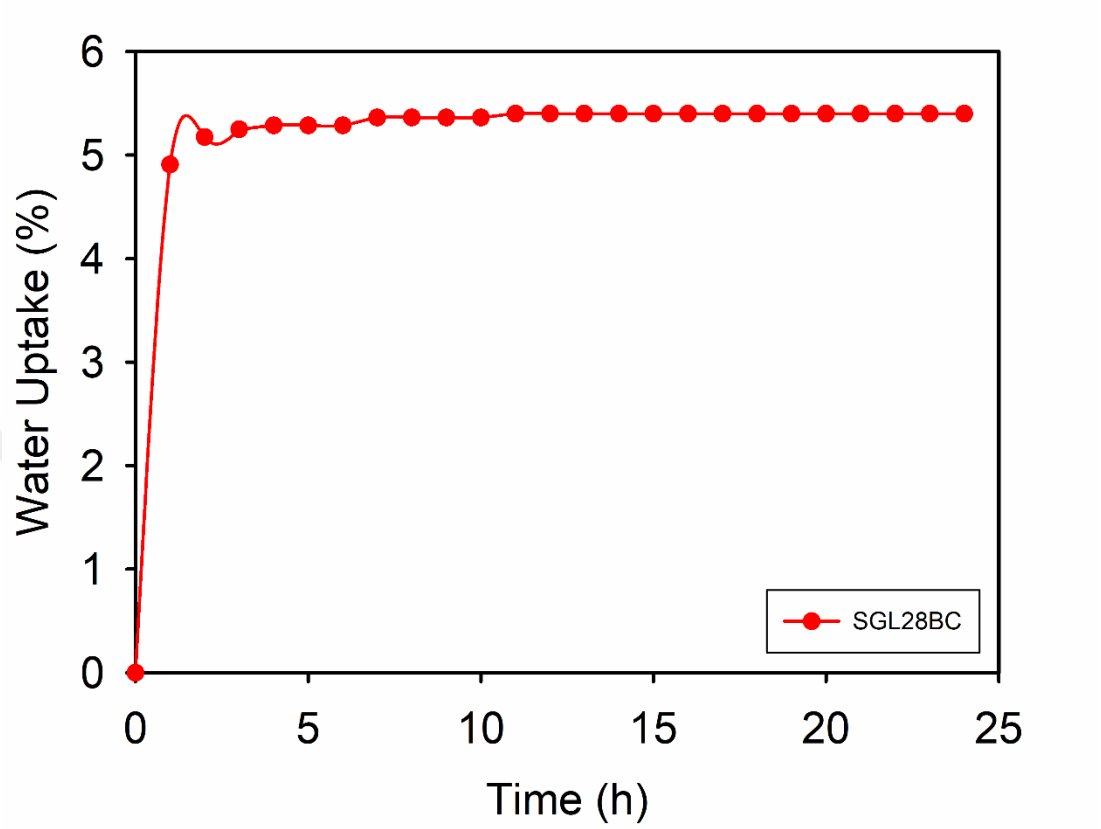

Figure 3.11 Water uptake of the SGL28BC

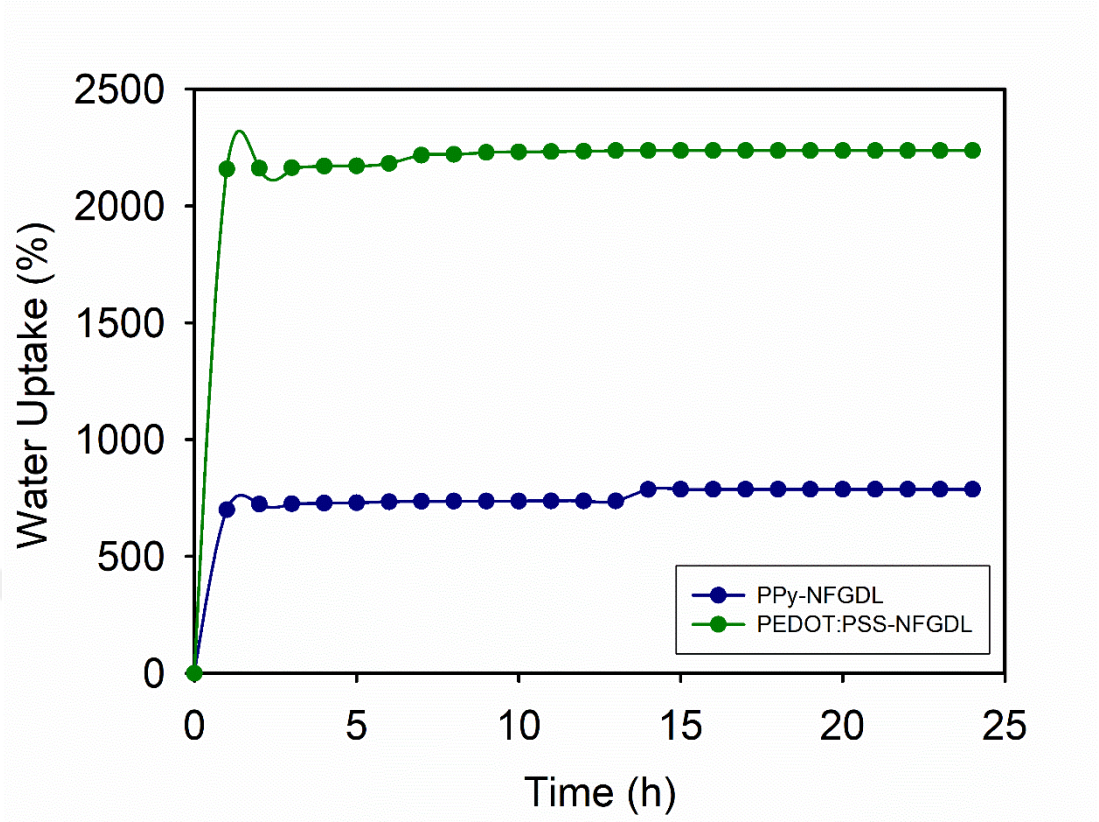

Figure 3.12 Water uptake of the PPy-NFGDL and PEDOT:PSS-NFGDL

The bulk porosity of SGL28BC, PPy-NFGDL and PEDOT:PSS-NFGDL after 10min and 24h immersion in water are given in Figure 3.13 and 3.14. According to these figures, the bulk porosity value of SGL28BC is the lowest for both immersion times. As can be seen from the SEM images previously given in Section 3.1 and Figure 3.2, the MPS at the surface of the GDL has inhomogeneous pores that are partially filled by PTFE. The MPL, on the other hand, completely covers the other surface of the GDL. Additionally, the applied hydrophobic PTFE also has a water-repellent effect. PPy-NFGDL has a lower bulk porosity than PEDOT:PSS-NFGDL. Moreover, after 24h of immersion, the bulk porosity of SGL28BC increases of 78% of its value at 10 min of immersion. For PPy-NFGDL, almost no variation is observed after 24h and an increase of 46% is observed after 24h for PEDOT:PSS-NFGDL. Therefore, it can be concluded that the highest dimentional stability is observed for the PPy-NFGDL. It is worth notice that the commercial GDL, SGL28BC presents the lowest bulk porosity but also the lowest dimensional stability in wet environment. In this context, the PPy-

NFGDL proposed is the most stable sample in terms of bulk porosity and dimensional stability.

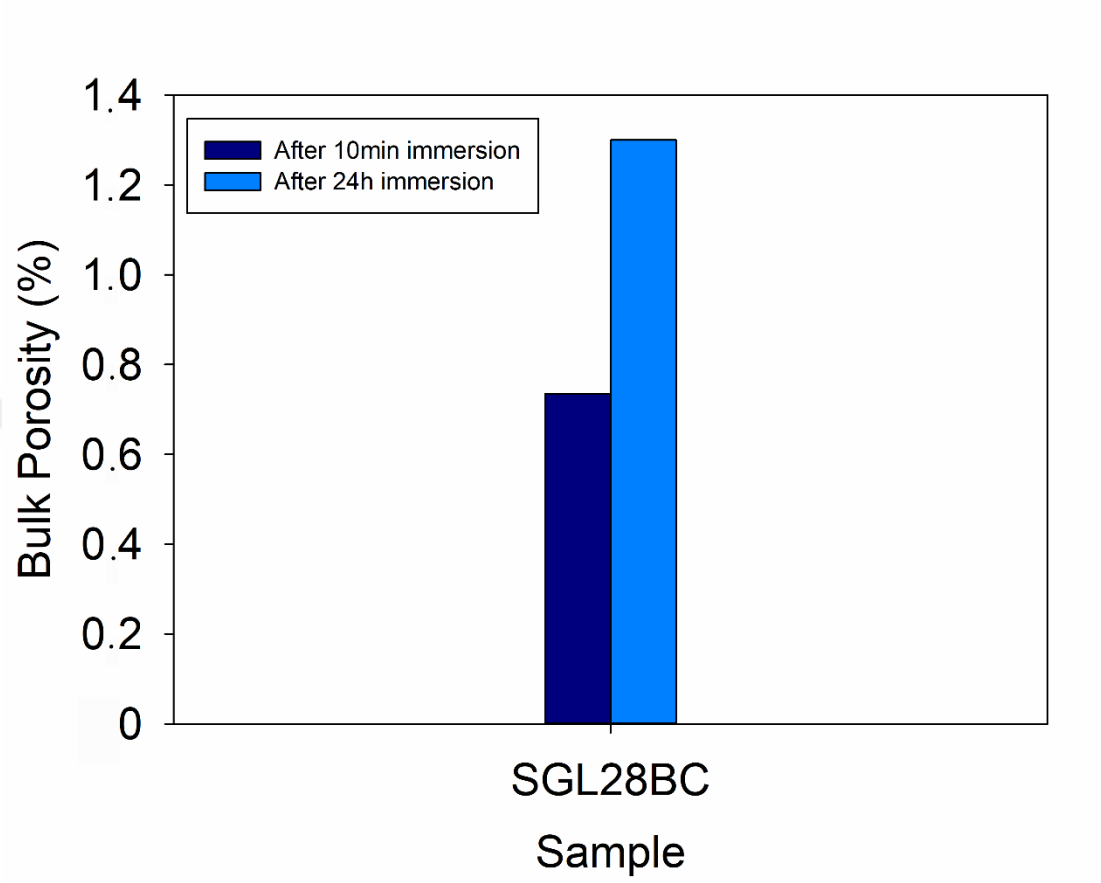

Figure 3.13 Bulk porosity of the SGL28BC commercial GDL

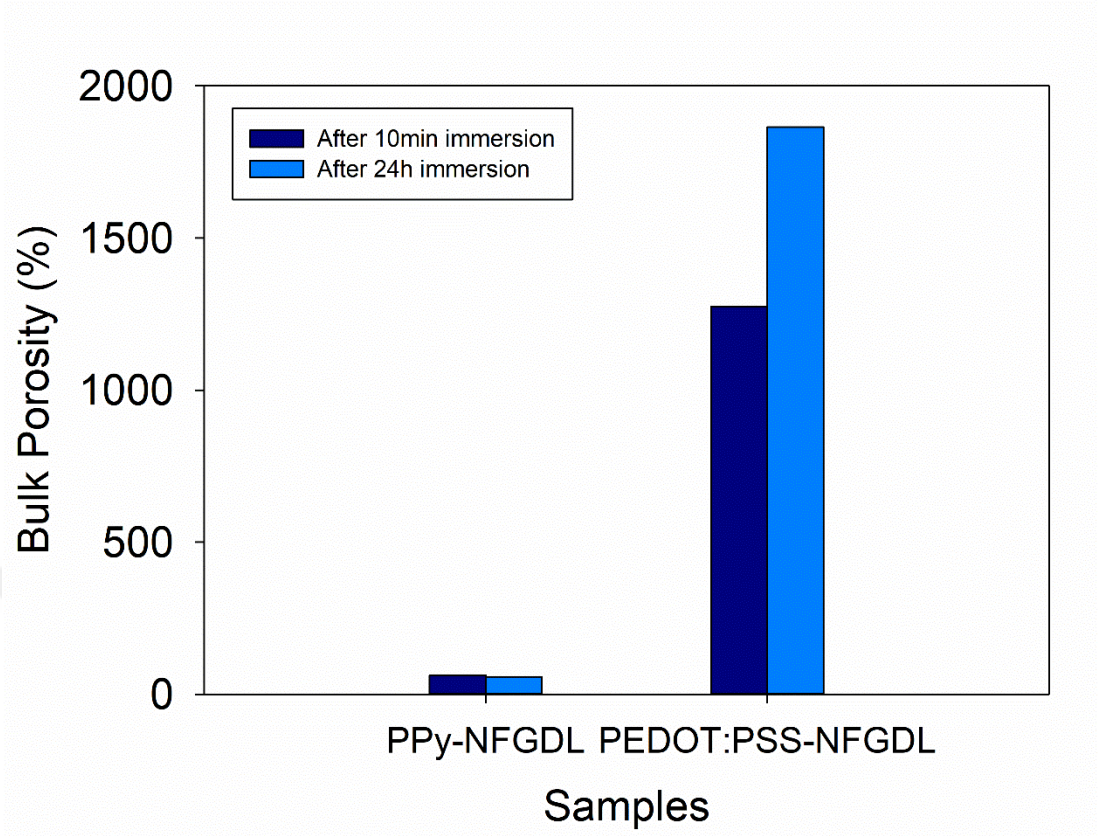

Figure 3.14 Bulk porosity of PPy-NFGDL and PEDOT:PSS-NFGDL

3.4 Electrical conductivity and performances in a fuel cell of the novel nanofiber GDLs

The electrical conductivity of the samples is gathered in Table 3.2. According to the results, PMMA has shown very low conductivity since it is an insulating material. When the insulating PMMA is coated with conjugated PPy and PEDOT:PSS, the conductivity obtained is approximately 23.0 and 207.0 $S.m^{-1}$, respectively. The commercial sample SGL28BC presents the highest conductivity. For this GDL the value provided by the manufacturer is also given. However, it is worth to notice that the manufacturer indicated that the GDL was compressed under 1MPa before measurement. Lower conductivities are obtained for novel nanofiber GDLs. Nevertheless, it is important to emphasize that electrical condcutivity results should be considered cautiously as all the samples considered are not bulk materials but porous materials. Therefore, the obtention of a uniform current flow required during the four

probe measurements is somewhat ambiguous for these materials and no clear conclusion can be drawn.

Table 3.2 Electrical conductivities of the samples

Samples	**Electrical conductivity (S/m)**
PMMA	5.7×10^{-6}
SGL28BC	5760.0
SGL28BC (Manufacturer) – compression at 1MPa	18000.0
PPy-NFGDL	23.0
PEDOT:PSS-NFGDL	207.0

As mentioned in the section 3.1, PEDOT:PSS-NFGDL underwent shrinkage during polymerization and became brittle. Therefore, cell performance tests were not performed with this sample. Figure 3.15 illustrates the current density values of SGL28BC and PPy-NFGDL measured at various voltages, along with the corresponding power densities. As it can be seen, the novel PPy-NFGDL exhibits a remarkable high performance getting nearly closer to the commercial GDL. An increasing current density is observed at decreasing voltage values and increasing current density up to a certain level also caused an increase in power density reaching a maximum value of 212.0 $mW.cm^{-2}$ and 150.0 $mW.cm^{-2}$ for SGL28BC and PPy-NFGDL, respectively. These results emphasizes that the prposed nanofiber GDLs are promising high performance and cheaper alternatives to traditional GDLs used in PEM fuel cells.

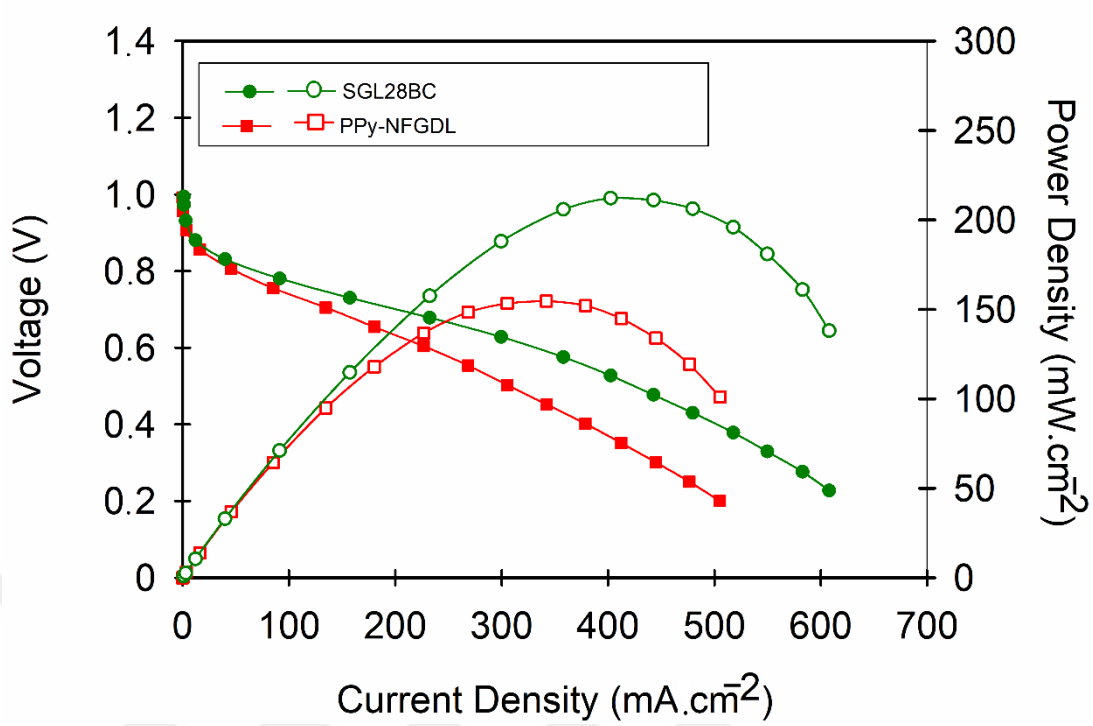

Figure 3.15 Polarization (filled symbols) and power density curves (empty symbols) of SGL28BC and PPy-NFGDL

CHAPTER 4

CONCLUSION

In conclusion, this study investigated the use of electrospun PMMA nanofibers coated with conductive PPy or PEDOT:PSS polymers as novel nanofiber GDL. Therefore, PMMA nanofiber layers were first electrospun with an applied voltage of 30 kV, a flow rate of 5 mL/h, and a needle tip-collector distance of 30 cm. The coating with conjugated polymers was realized by chemical oxidative polymerization. Based on the comprehensive analysis of the samples, several key conclusions can be drawn regarding their structural characteristics and performance metrics.

PPy-NFGDL layer with a thickness of 445µm and composed of PPy-coated PMMA nanofibers of around 700nm and nearly 50µm thick PEDOT:PSS-NFGDL layer made of PEDOT:PSS coated PMMA nanofibers of 720nm where produced. SEM-EDS analysis showed that PPy particularly polymerized and covered the whole surface of PMMA nanofibers without obstructing the pores. PPy adhered perfectly to the surface of PMMA nanofibers and no gaps or voids were observed at the interface. On the other hand, PEDOT:PSS polymerized as a matrix around the nanofibers but also in the pores and do not adhere perfectly to PMMA as SEM analysis revealed voids at the interface between the two polymers.

Although PPy-NFGDL layer was somewhat flexible and remained intact after drying, PEDOT:PSS-NFGDL was brittle and presented shrinkage after drying. This phenomenon was attributed to the shrinkage of the PSS chain segments composing the conductive polymer. This point will be improved in future studies by the use of plasticizer.

Moreover, the bulk porosity measurements at 24h water immersion also revealed that no dimensional variation was observed for the novel PPy-NFGDL. Therefore, it presents a better dimensional stability in wet conditions compared to the commercial GDL and PEDOT:PSS for which the porosity increased of 78% and 46%, respectively.

Although the electrical conductivity of nanofiber GDLs seems relatively lower than that of the commertial specimen, a noticeably high performance was achieved by the novel PPy-NFGDL. A power density as high as 150 $mW.cm^{-2}$ was measured. Overall, these findings underscore the diverse structural attributes and performance characteristics of the NFGDLs, each offering unique advantages and suitability for different applications depending on their specific conductivity, thickness, porosity, and dimensional stability requirements. This investigation represents a novel approach in the field, as no similar study has been reported in the literature. It eliminates the need for traditional MPL and MPS layers and demonstrates the feasibility of producing eco-friendly high performance NFGDLs solely from a nanofibers coated with conjugated polymers.

4.1 Perspectives

In the present study, the high efficiency achieved with PPy-NFGDL featuring low conductivity values suggests potential for enhancement through optimization efforts such as increasing the conjugated polymer ratio or producing the sample in a more bulk structure. Also, the voids observed in PEDOT:PSS coated PMMA nanofibers are attributed to inadequate adhesion between the PEDOT:PSS and PMMA. Addressing this issue could involve enhancing the polymer coating process or exploring alternative polymerization techniques to achieve better adhesion. Additionally, issues of shrinkage and brittleness in PEDOT:PSS-NFGDL could be mitigated by incorporating plasticizer**.** There are studies in the literature that mention the use of plasticizer [86]. Consequently, fuel cell performance evaluation of PEDOT:PSS-NFGDL becomes feasible. Future investigations could delve deeper into optimizing these materials for industrial applications and their integration into emerging technologies such as energy storage systems.

REFERENCES

[1] Supapo, K. R. M., Lozano, L., Tabañag, I. D. F. & Querikiol, E. M. A Geospatial Approach to Energy Planning in Aid of Just Energy Transition in Small Island Communities in the Philippines. Applied Sciences, *11*(24), 11955. 2021.

[2] Strielkowski, W., Civin, L., Tarkhanova, E., Tvaronavičienė, M. & Petrenko, Y., Renewable Energy in the Sustainable Development of Electrical Power Sector: A Review. Energies, *14*(24), 8240. 2021.

[3] Shanbhag, D. T. The Ozone Layer, Ultraviolet B Radiation, Climate Change and Human Health. Environmental Change and Public Health. Inesa Ventures. 2022.

[4] Hartley, H. Michael Faraday as a physical chemist. Transactions of the Faraday Society, *49*, 473-488. 1953.

[5] Bıyıkoğlu, A. Yakıt Hücrelerinin Tarihsel Gelişimi, Çalışma Prensipleri ve Bugünkü Durumu. G.Ü. Fen Bilimleri Dergisi, *16*(3), 523-542. 2003.

[6] Appleby, A. From Sir William Grove to today: fuel cells and the future. Journal of Power Sources, *29*(1-2), 3-11. 1990.

[7] Kirubakaran, A., Jain, S. & Nema, R. A review on fuel cell technologies and power electronic interface. Renewable and Sustainable Energy Reviews, *13*(9), 2430-2440. 2009.

[8] Fan, L., Tu, Z. & Chan, S. H. Recent development of hydrogen and fuel cell technologies: A review. Energy Reports, *7*, 8421-8446. 2021.

[9] Roth, W., Benz, J., Ortiz, B. & Sauer, D. U. Fuel cells in photovoltaic hybrid systems for stand-alone power supplies. 2003.

[10] Innovation, A. F. C. *Types of fuel cells.* Retrieved 2023, from http://www.antig.com/technology/technology_fuel_cell_types.htm.

[11] Corbo, P., Migliardini, F. & Veneri, O. Performance investigation of 2.4 kW PEM fuel cell stack in vehicles. International Journal of Hydrogen Energy, *32*(17), 4340-4349. 2007.

[12] Wu, B., Matian, M. & Offer, G. J. Hydrogen PEMFC system for automotive applications. International Journal of Low-Carbon Technologies, *7*(1), 28-37. 2012.

[13] Yalcinoz, T. & Alam, M. Improved dynamic performance of hybrid PEM fuel cells and ultracapacitors for portable applications. International Journal of Hydrogen Energy, *33*(7), 1932-1940. 2008.

[14] Devrim, Y., Devrim, H. & Eroglu, I. Development of 500 W PEM fuel cell stack for portable power generators. International Journal of Hydrogen Energy, *40*(24), 7707-7719.

[15] Venturelli, L., Santangelo, P. E. & Tartarini, P. Fuel cell systems and traditional technologies. Part II: Experimental study on dynamic behavior of PEMFC in stationary power generation. Applied Thermal Engineering, *29*(17-18), 3469-3475. 2009.

[16] Niestrój, R., Rogala, T. & Skarka, W. An Energy Consumption Model for Designing an AGV Energy Storage System with a PEMFC Stack. Energies, *13*(13), 3435. 2020.

[17] Gong, M., Zhang, X., Chen, M. & Ren, Y. Proton Exchange Membrane Fuel Cell as an Alternative to the Internal Combustion Engine for Emission Reduction: A Review on the Effect of Gas Flow Channel Structures. Atmosphere, *14*(3), 439. 2023.

[18] Duan, Y., Liu, H., Zhang, W., Khotseng, L., Xu, Q. & Su, H. Materials, components, assembly and performance of flexible polymer electrolyte membrane fuel cell: A review. Journal of Power Sources, *555*, 232369. 2023.

[19] Guo, H., Chen, L., Ismail, S. A., Jiang, L., Guo, S., Gu, J., Zhang, X., Li, Y., Zhu, Y., Zhang, Z. & Han, D. Gas Diffusion Layer for Proton Exchange Membrane Fuel Cells: A Review. Materials, *15*(24), 8800. 2022.

[20] Mercuri, R. A. & Gough, J. J. Flexible graphite composite for use in the form of a fuel cell flow field plate. US Patent, *111*,139. 2000.

[21] Reiser, C. & Sawyer, R. Solid polymer electrolyte fuel cell stack water management system. US Patent, 4769297. 1988.

[22] Wilson, M. S. & Zawodzinski, C. Fuel cell with metal screen flow-field. US Patent, 5798187. 1998.

[23] Voss, H. H. & Chow, C. Y. Coolant flow field plate for electrochemical fuel cells. US Patent, *5*,230,966. 1993.

[24] Wilkinson, D. P., Lamont, G. J., Voss, H. H. & Schwab, C. Embossed fluid flow field plate for electrochemical fuel cells. US Patent, *5*,521,018. 1996.

[25] Washington, K. B., Wilkinson, D. P. & Voss, H. H. Laminated fluid flow field assembly for electrochemical fuel cells. US Patent, *5*,300,370. 1994.

[26] Ernst, W. D. & Mittleman, G. PEM-type fuel cell assembly having multiple parallel fuel cell sub-stacks employing shared fluid plate assemblies and shared membrane electrode assemblies. US Patent, *5*,945,232. 1999.

[27] Yoshiake, A. Solid polymer electrolyte fuel cell. US Patent, 1999.

[28] Shen, J., Tu, Z. & Chan, S. H. Performance enhancement in a proton exchange membrane fuel cell with a novel 3D flow field. Applied Thermal Engineering, *164*, 114464. 2020.

[29] Ahn, C.Y., Cheon, J.Y., Joo, S.H. & Kim, J. Effects of ionomer content on Pt catalyst/ordered mesoporous carbon support in polymer electrolyte membrane fuel cells. Journal of Power Sources, *222*(15), 477-482. 2013.

[30] Barbir, F., *Fuel Cells Theory and Practice.* Elsevier. 2013.

[31] Athanasaki, G., Jayakumar, A. & Kannan, A. Gas diffusion layers for PEM fuel cells: Materials, properties and manufacturing – A review. International Journal of Hydrogen Energy, *48*(6), 2294-2313. 2023.

[32] Zaarour, B., Zhu, L. & Jin, X. A Review on the Secondary Surface Morphology of Electrospun Nanofibers: Formation Mechanisms, Characterizations, and Applications. Chemistry Select, *5*(4), 1335-1348. 2020.

[33] Begum, H. A. & Khan, M. International Journal of Textile Science, *6*, 110-117. 2017.

[34] Li, Z. & Wang, C. Effects of Working Parameters on Electrospinning. One-Dimensional Nanostructures, 15-28. 2013.

[35] Akkoyun, S. & Öktem, N. Effect of viscoelasticity in polymer nanofiber electrospinning: Simulation using FENE-CR model. Engineering Science and Technology, an International Journal, *24*, 620-630. 2021.

[36] Yuan, D. X., Zhang, Y., Dong, C. & Sheng, J. Morphology of ultrafine polysulfone fibers prepared by electrospinning. Polymer International, *53*(11), 1704-1710. 2004.

[37] Acik, G., Cansoy, C. E. & Kamaci, M. Effect of flow rate on wetting and optical properties of electrospun poly(vinyl acetate) micro-fibers. Colloid and Polymer Science, *297,* 77-83. 2019.

[38] Zhu, J., Yan, C., Li, G., Cheng, H., Li, Y., Liu, T., Mao, Q., Cho, H., Gao, Q., Gao, C., Jiang, M., Dong, X. & Zhang, X. Recent developments of electrospun nanofibers for electrochemical energy storage and conversion. Energy Storage Materials, *65*, 103111. 2023.

[39] Bae H. S., Haider A., Selim K. M. K., Kang D. Y., Kim E. J., & Kang I. K. Fabrication of highly porous PMMA electrospun fibers and their application in the removal of phenol and iodine. Journal of Polymer Research, *20*, 1-7. 2013.

[40] Tavakkol, E., Tavanai, H., Abdolmaleki, A. & Morshed, M. Production of conductive electrospun polypyrrole/poly(vinyl pyrrolidone) nanofibers. Synthetic Metals, *231*, 95-106. 2017.

[41] Zhang, Y., Ouyang, H., Lim, C. T., Ramakrishna, S. & Huang, Z.-M. Electrospinning of gelatin fibers and gelatin/PCL composite fibrous scaffolds. Journal of Biomedical Materials Research Part B: Applied Biomaterials, *72*(1), 156-165. 2004.

[42] Dasdemir, M., Topalbekiroglu, M. & Demir, A. Electrospinning of thermoplastic polyurethane microfibers and nanofibers from polymer solution and melt. Journal of Applied Polymer Science, *127*(3), 1901-1908. 2012.

[43] Choi, S.-S., Lee, Y. S., Joo, C. W., Lee, S. G., Park, J. K. & Han, K.-S. Electrospun PVDF nanofiber web as polymer electrolyte or separator. Electrochimica Acta, *50*(2-3), 339-343. 2004.

[44] Alwan, T. J., Toma, Z. A., Kudhier, M. A. & Ziadan, K. M. Preparation and Characterization of the PVA Nanofibers Produced By Electrospinning. Journal of Nanotechnology & Nanoscience, *1*(1), 1-3. 2016.

[45] Kim, W.-T., Park, D.-C., Yang, W.-H., Cho, C.-H. & Choi, W.-Y. Effects of Electrospinning Parameters on the Microstructure of PVP/TiO2 Nanofibers. Nanomaterials, *11*(6), 1616. 2021.

[46] Matulevicius, J., Kliucininkas, L., Martuzevicius, D., Krugly, E., Tichonovas, M. & Baltrusaitis, J. Design and Characterization of Electrospun Polyamide Nanofiber Media for Air Filtration Applications. Journal of Nanomaterials, *1*, 859656. 2014.

[47] Ma, H., Burger, C., Hsiao, B. S. & Chu, B. Ultra-fine cellulose nanofibers: new nano-scale materials for water purification. Journal of Materials Chemistry, *21*, 7507-7510. 2011.

[48] Mbese, Z., Alven, S. & Aderibigbe, B. A. Collagen-Based Nanofibers for Skin Regeneration and Wound Dressing Applications. Polymers, *13*(24), 4368. 2021.

[49] Ji, L., Lin, Z., Medford, A. J. & Zhang, X. Porous carbon nanofibers from electrospun polyacrylonitrile/SiO2 composites as an energy storage material. Carbon, *47*(14), 3346-3354. 2009.

[50] Bagherzadeh, R., Latifi, M., Najar, S. S., Tehran, M. A., Gorji, M. & Kong, L. Transport properties of multi-layer fabric based on electrospun nanofiber mats as a breathable barrier textile material. Textile Research Journal, *82*(1), 70-76. 2011.

[51] Wang, Q., Yan, S., Han, G., Li, X., You, R., Zhang, Q., Li, M. & Kaplan, D. L. Facile production of natural silk nanofibers for electronic device applications. Composites Science and Technology, *187*, 107950. 2020.

[52] Virji, S., Huang, J., Kaner, R. B. & Weiller, B. H. Polyaniline Nanofiber Gas Sensors: Examination of Response Mechanisms. Nano Letters, *4*(3), 491-496. 2004.

[53] Ito, T., Shirakawa, H. & Ikeda, S. Simultaneous polymerization and formation of polyacetylene film on the surface of concentrated soluble Ziegler-type catalyst solution. Journal of Polymer Science: Polymer Chemistry Edition, *12*(1), 11-20. 1974.

[54] Shirakawa, H., Louis, E. J., MacDiarmid, A. G., Chiang, C. K. & Heeger, A. J. Synthesis of electrically conducting organic polymers: halogen derivatives of polyacetylene, (CH)x. Journal of the Chemical Society, Chemical Communications, *16*, 578-580. 1977.

[55] The Nobel Prize in Chemistry 2000. Retrieved 2024, from https://www.nobelprize.org/prizes/chemistry/2000/summary/.

[56] Saçak, P. D. M. "Polimer Kimyası", Gazi Kitabevi, 2023.

[57] Rasmussen, S. C. On the Origin of 'Synthetic Metals': Herbert McCoy, Alfred Ubbelohde, and the Development of Metals from Nonmetallic Eléments. Bulletin for the History of Chemistry, *41*(1-2), 64-73. 2016.

[58] Han, J.-J., Zhang, N., Li, D.-L., Han, H. M. T. & Sun, D.-D. Cyclic voltammetry for the determination of the selectivity of PANI-HClO4 sensor to different acids. Ionics, *26*, 1029-1038. 2019.

[59] Gursoy, O., Gursoy, S. S., Cogal, S. & Cogal, G. C. Development of a new two-enzyme biosensor based on poly(pyrrole-co-3,4-ethylenedioxythiophene) for lactose determination in milk. Polymer Engineering & Science, *58*(6), 839-848. 2017.

[60] Chulkin, P. & Łapkowski, M. An Insight into Ionic Conductivity of Polyaniline Thin Films. Materials, *13*(12). 2020.

[61] Ji, S., Yang, J., Cao, J., Zhao, X., Mohammed, M. A., Dryfe, R. A. W. & Kinloch, I. A. A Universal Electrolyte Formulation for the Electrodeposition of Pristine Carbon and Polypyrrole Composites for Supercapacitors. ACS Applied Materials & Interfaces, *12*(11). 2020.

[62] Mathew, S. & Thomas, P. C. Fabrication of polyaniline nanocomposites as electrode material for power generation in microbial fuel cells. Materials Today: Proceedings, *33*, 1415-1419. 2020.

[63] Attar, A. E., Oularbi, L., Chemchoub, S. & Rhazi, M. E. Preparation and characterization of copper oxide particles/polypyrrole (Cu2O/PPy) via electrochemical method: Application in direct ethanol fuel cell. International Journal of Hydrogen Energy, *45*(15), 8887-8898. 2020.

[64] Carli, S., Fioravanti, G., Armirotti, A., Ciarpella, F., Prato, M., Ottonello, G., Salerno, M., Scarpellini, A., Perrone, D., Marchesi, E., Ricci, D. & Fadiga, L. A New Drug Delivery System based on Tauroursodeoxycholic Acid and PEDOT. Chemistry - A European Journal, *25*(9). 2018.

[65] Hao, L., Dong, C., Zhang, L., Zhu, K. & Yu, D. Polypyrrole Nanomaterials: Structure, Preparation and Application. Polymers, *14*(23), 5139. 2022.

[66] Groenendaal, L., Zotti, G., Aubert, P., Waybright, S. M. & Reynolds, J. Electrochemistry of Poly(3,4-alkylenedioxythiophene) Derivatives Advanced Materials, *15*(11), 854-879. 2003.

[67] O'Kane D. M., "What is PEDOT:PSS?," Retrieved 2024, from https://www.ossila.com/pages/what-is-pedot-pss.

[68] Merlini, C., Barra, G. M. O., Araujo, T. M. & Pegoretti, A. Electrically pressure sensitive poly(vinylidene fluoride)/polypyrrole electrospun mats. RSC Advances, *30*(4), 15749-15758. 2014.

[69] Choi, J., Lee, J., Choi, J., Jung, D. & Shim, S. E. Electrospun PEDOT/PVP nanofibers as the chemiresistor in chemical vapour sensing. Synthetic Metals, *160*(13-14), 1415-1421. 2010.

[70] Bonakdar, M. A. & Rodrigue, D. Electrospinning: Processes, Structures, and Materials. Macromol, *4*(1), 58-103. 2024.

[71] Khatti, T., Naderi-Manesh, H. & Kalantar, S. M. Polypyrrole-Coated Polycaprolactone-Gelatin Conductive Nanofibers: Fabrication and Characterization. Materials Science & Engineering B, *250*. 2019.

[72] Sakunpongpitiporn, P., Phasuksom, K., Paradee, N. & Sirivat, A. Facile synthesis of highly conductive PEDOT:PSS via surfactant templates. RSC Advances, *9*, 6363–6378. 2019.

[73] Kord, B., Ismaeilimoghadam, S. & Malekian, B. Effect of immersion temperature on the water uptake of polypropylene/wood flour/organoclay hybrid nanocomposite. BioResources, *6*(1), 584-593. 2011.

[74] Xie, A., Cui, J., Yang, J., Chen, Y., Lang, J., Li, C., Yan, Y. & Dai, J. Photo-Fenton self-cleaning PVDF/NH2-MIL-88B(Fe) membranes towards highly-

efficient oil/water emulsion separation. Journal of Membrane Science, *595*, 117499. 2020.

[75] Sun, L., Cai, Y., Kim, D., Kim, S., Zhu, C., Wang, F., Ullah, A., Wong, P. Y., Mayakrishnan, G., Lee, C. & Kim, I. S. Enhanced properties of solid polymer electrolytes by a bilayer nonwoven PET/nanofiber PVDF substrate for use in all-solid-state lithium metal batteries. Journal of Power Sources, *564*, 232851. 2023.

[76] Valtakari, D., Liu, J., Kumar, V., Xu, C., Toivakka, M. & Saarinen, J. J. Conductivity of PEDOT on Spin-Coated and Drop Cast Nanofibrillar Cellulose Thin Films. Nanoscale Research Letters, *10*, 386. 2015.

[77] Carter, J. L., Kelly, C. A. & Jenkins, M. J. Processing optimization of PEDOT and PEDOT/Tween 80 films. Polymer Journal, *55*(253-260), 1-10. 2023.

[78] Koidis, C., Logothetidis, S., Kapnopoulos, C., Karagiannidis, P. G., Laskarakis, A., & Hastas, N. A. Substrate treatment and drying conditions effect on the properties of roll-to-roll gravure printed PEDOT: PSS thin films. Materials Science and Engineering: B, *176*(19), 1556-1561. (2011).

[79] Friedel, B., Keivanidis, P. E., Brenner, T. J., Abrusci, A., McNeill, C. R., Friend, R. H., & Greenham, N. C. Effects of layer thickness and annealing of PEDOT: PSS layers in organic photodetectors. Macromolecules, *42*(17), 6741-6747. (2009).

[80] Carrigy, N. B., Pant, L. M., Mitra, S. & Secanell, M. Knudsen Diffusivity and Permeability of PEMFC Microporous Coated Gas Diffusion Layers for Different Polytetrafluoroethylene Loadings. Journal of The Electrochemical Society, *160*(2), 81-89. 2013.

[81] Pepe, Y., Akkoyun, S., Bozkurt, B., Karatay, A., Ates, A. & Elmali, A. One-photon absorption enhanced nonlinear absorption and optical limiting of the electrospun polyvinylpyrrolidone via excitation energy and incorporation of

polypyrrole particles. Journal of Materials Science, *57*(19), 21265-21275. 2022.

[82] Oroumei, A., Tavanai, H. & Morshed, M. Electrical resistance and heat generation of polypyrrole-coated polyacrylonitrile nanofibrous and regular fibrous mats. Polymers for Advanced Technologies, *23*(9), 1302-1310. 2011.

[83] Morgan, J. M. & Datta, R. Understanding the gas diffusion layer in proton exchange membrane fuel cells. I. How its structural characteristics affect diffusion and performance. Journal of Power Sources, *251*, 269-278. 2014.

[84] Najaf, S. K., Tajvidi, M. & Hamidina, E. Effect of temperature, plastic type and virginity on the water uptake of sawdust/plastic composites. Holz Roh Werkst, *65*(5), 377-382. 2007.

[85] Isloor, A. M., Pereira, V. R., Bhat, B. U. & Al-Obaid, A. M. Preparation and performance studies of Polysulfone-Sulfated nano-Titania (S-TiO2) nanofiltration membranes for dye removal. RSC Advances, *5*(66), 54053-54061. 2015.

[86] Fan, X., Nie, W., Tsai, H., Wang, N., Huang, H., Cheng, Y., Wen, R., Ma, L., Yan, F. & Xia, Y. PEDOT for Flexible and Stretchable Electronics: Modifications, Strategies, and Applications. Advanced Science, *6*(19), 1900625. 2019.

CURRICULUM VITAE

PERSONAL INFORMATION

Name Surname **:** Nurcan AŞÇI
Date of Birth **:**
Phone **:**
E-mail :

EDUCATION

High School **:** Çankaya Sancak Anatolian High School (2012-2016)
Bachelor **:** Ankara Yıldırım Beyazıt University (2016-2021)
Master Degree **:** Ankara Yıldırım Beyazıt University (2022-continued)

WORK EXPERIENCE

Research and Development Engineer : Sunlego Enerji Sistemleri A.Ş. (2024-continued)

TOPICS OF INTEREST

Polymer materials, polymer nanofibers, proton exchange membrane fuel cells, gas diffusion layers, electrospinning.

PUBLICATIONS

Pepe, Y., Akkoyun, S., Asci, N., Cevik, E., Tutel, Y., Karatay, A., ... & Elmali, A. Investigation of the Defect and Intensity-Dependent Optical Limiting Performance of MnO2 Nanoparticle-Filled Polyvinylpyrrolidone Composite Nanofibers. ACS omega, 8(50), 47954-47963, 2023.

Pepe, Y., Tutel, Y., Akkoyun, S., Asci, N., Cevik, E., Karatay, A., ... & Elmali, A. Visible-light optical limiting of vanadia–polyvinylpyrrolidone nanofibers. Journal of Materials Science, 59(10), 4102-4117, 2024.

Pepe, Y., Akkoyun, S., Asci, N., Cakır, O., Tutel, Y., Unalan, H. E., ... & Elmali, A. Tungsten oxide filled nanofibers for optical limiting in near infrared region. Optics & Laser Technology, 176, 110970, 2024.

Pepe, Y., Tutel, Y., Akkoyun, S., Asci, N., Cevik, E., Karatay, A., ... & Elmali, A. Enhanced Nonlinear Optical Limiter in the Visible Spectral Region Based on Fe-and Co-Doped NiO Nanoparticles within PVP Nanofibers. ACS Applied Nano Materials, 2024.

PRESENT ORGANIZED SOURCES / PRESENTATION

3rd International Congress on Scientific Advances, 12.2023, Turkey, Application of polypyrrole containing polyvinylpyrrolidone nanofibers as microporous layer on commercial gas diffusion layers for PEM fuel cells.

9th International Advanced Technologies Symposium, 10.2021, Turkey, Fabrication and Characterization of Electrospun Thermoplastic Polyurethane Nanofibers and Polyvinylpyrrolidone/Aloe Vera Hydrogel Sandwich Structure.